

# Colloidal Self-Assembly Concepts for Plasmonic Metasurfaces

Martin Mayer, Max J. Schnepf, Tobias A. F. König,\* and Andreas Fery\*

**Metallic nanostructures exhibit strong interactions with electromagnetic radiation, known as the localized surface plasmon resonance. In recent years, there is significant interest and growth in the area of coupled metallic nanostructures. In such assemblies, short- and long-range coupling effects can be tailored and emergent properties, e.g., metamaterial effects, can be realized. The term “plasmonic metasurfaces” is used for this novel class of assemblies deposited on planar surfaces. Herein, the focus is on plasmonic metasurfaces formed from colloidal particles. These are formed by self-assembly and can meet the demands of low-cost manufacturing of large-area, flexible, and ultrathin devices. The advances in high optical quality of the colloidal building blocks and methods for controlling their self-assembly on surfaces will lead to novel functional devices for dynamic light modulators, pulse sharpening, subwavelength imaging, sensing, and quantum devices. This progress report focuses on predicting optical properties of single colloidal building blocks and their assemblies, wet-chemical synthesis, and directed self-assembly of colloidal particles. The report concludes with a discussion of the perspectives toward expanding the colloidal plasmonic metasurfaces concept by integrating them with quantum emitters (gain materials) or mechanically responsive structures.**

## 1. Introduction

In metallic thin films, light can drive coherent oscillations of the free electrons at the metal–dielectric interface. This

M. Mayer, M. J. Schnepf, Dr. T. A. F. König, Prof. A. Fery  
 Leibniz-Institut für Polymerforschung Dresden e.V. (IPF)  
 Institute for Physical Chemistry and Polymer Physics  
 Hohe Str. 6, 01069 Dresden, Germany  
 E-mail: koenig@ipfdd.de; fery@ipfdd.de

M. Mayer, Dr. T. A. F. König, Prof. A. Fery  
 Cluster of Excellence Center for Advancing Electronics Dresden (cfaed)  
 Technische Universität Dresden  
 Helmholtzstraße 18, 01069 Dresden, Germany  
 Prof. A. Fery  
 Physical Chemistry of Polymeric Materials  
 Technische Universität Dresden  
 Bergstraße 66, 01069 Dresden, Germany

 The ORCID identification number(s) for the author(s) of this article can be found under <https://doi.org/10.1002/adom.201800564>.

© 2018 The Authors. Published by WILEY-VCH Verlag GmbH & Co. KGaA, Weinheim. This is an open access article under the terms of the Creative Commons Attribution-NonCommercial-NoDerivs License, which permits use and distribution in any medium, provided the original work is properly cited, the use is non-commercial and no modifications or adaptations are made.

The copyright line of this paper was changed on 26 October 2018 after initial publication.

DOI: 10.1002/adom.201800564

oscillation, known as a surface plasmon resonance, depends on specific wavelength, polarization, and angle of incidence of the light as well as the thickness of the metallic thin film.<sup>[1]</sup> Less precision is needed to reach the resonance conditions for spherical metallic nanoparticles, for which the excitation wavelength must be much larger than the particle diameter.<sup>[2]</sup> Because of the localization of the oscillation within nanoparticles, surface plasmon resonances allow for localization of electromagnetic field below the diffraction limit.<sup>[3]</sup> Furthermore, the scattering and absorption properties of plasmonic nanoparticles can be tailored by controlling their composition, size, geometry, and environment.<sup>[4]</sup> These special properties of plasmonic nanoparticles stimulated growing interest in a variety of applications, including coloring agents (e.g., plasmonic windows<sup>[5]</sup>) electronics (e.g., plasmonic solar cells<sup>[6]</sup>), optics (e.g., resolution below diffracting limit<sup>[7]</sup>), medicine (e.g., cancer treatment<sup>[8]</sup>), and sensors

(signal/sensitivity enhancement<sup>[9]</sup>). Although these effects are obvious in isolated, individual plasmonic nanoparticles. The plasmonic coupling of metallic nanoparticles in assemblies can be controlled and imparts tunable interactions with electromagnetic radiation and new, emergent properties. Examples include a dramatic color change when varying the distance between coupled nanoparticles,<sup>[10]</sup> strong electromagnetic field enhancement,<sup>[11]</sup> and hybridized plasmon modes.<sup>[12]</sup> Simply assembling nanoparticles into dimers can result in superior field enhancement and improved sensitivity in Raman scattering spectroscopy.<sup>[13]</sup> Moreover, advancements in theory, simulations, and computing power have facilitated the rational design of complex nanoparticles and well-defined assemblies.<sup>[14]</sup>

Plasmonic metasurfaces are assemblies of plasmonic nanostructures deposited on surfaces. The reduction to two dimensions has a decisive advantage that the exceptional abilities for controlling the flow of light can be integrated in planar, scalable and low-cost manufacturing processes.<sup>[15]</sup> With proper control and design of the local and long-range coupling effects, novel and useful properties, beyond the behavior of single nanoparticles, can emerge. These properties include the capability to manipulate amplitude, phase, and polarization of light<sup>[16]</sup> at subwavelength resolution,<sup>[17]</sup> intense electric field enhancement in hot-spots between nanoparticles,<sup>[9]</sup> and an effective negative index of refraction for a particular wavelength for some types of hierarchical assemblies.<sup>[18]</sup> These mentioned concepts can be further exploited to target imaging below the diffraction

limit (superlenses)<sup>[19]</sup> and ultrathin invisibility skin cloaks.<sup>[20]</sup> The general term, “plasmonic metasurface,” is not defined in the literature in the strict sense of the classical metamaterial definition of Cai and Shalaev. “A metamaterial is an artificial structured material, which attains its properties from the unit structure rather than the constituent materials. A metamaterial has an inhomogeneity scale that is much smaller than the wavelength of interest, and its electromagnetic response is expressed in terms of homogenized material parameters.”<sup>[21]</sup> Rather, the phenomenon of emergent properties is used as the defining element.<sup>[15]</sup>

Despite the excellent potential for applications, there have been few practical demonstrations of plasmonic metasurfaces. Applications are often hampered by the limited scalability of the available fabrication techniques. Approaches for designing and functionalizing colloidal nanoparticles that allow for controlled self-assembly and the fabrication of monolayers with macroscopic dimensions are therefore critically important for advancing the field. These concepts enable programmability of the self-assembled metasurface, scalability, and reproducibility.<sup>[6]</sup> Moreover, plasmonic nanoparticles of high optical quality arising from their homogenous sizes and shapes and defined crystallinity can be obtained from wet-chemical synthesis techniques, including seeded growth.<sup>[22]</sup>

In the following sections, we discuss steps in rationally designing and realizing colloid-based plasmonic metasurfaces. We begin with the structure–property relationships of single nanoparticles, followed by a discussion of interactions between plasmonic nanoparticles and their interactions with surfaces. Precise requirements for the design of plasmonic metasurfaces complement the state-of-the-art techniques for wet-chemical synthesis and colloidal assembly. Finally, we extend the scalable colloidal metasurface concept to responsive and functional metasurfaces through integration with gain and mechanosensitive materials.

## 2. Electromagnetic Modeling and Wet-Chemical Synthesis to Fabricate Colloidal Plasmonic Metasurfaces

### 2.1. Optical Properties and Synthesis of Plasmonic Particles

In this section, we introduce the design rules and experimental approaches for tailoring the optical properties of isolated, noninteracting nanoparticles. The theory presented has been selected to align with the types and properties of nanoparticles that are readily obtained through wet-chemical synthesis. Therefore, the reader is guided in the choice of optical properties and synthetic methods.

The optical response of an isolated nanoparticle is the starting point toward designing complex assemblies. **Figure 1** shows the design principles of plasmonic building blocks and their correlated optical response, as summarized in the following rules: Increasing the diameter of the nanoparticle causes (1) a redshift in the surface plasmon resonance (to lower energy) and (2) an increase in the effective absorption cross-section. Mie theory calculations of spherical gold particle with



**Tobias A. F. König** is an independent research group leader in the Department of Nanostructured Materials at the Leibniz Institute of Polymer Research, Dresden and in the Department of Physical Chemistry at the Technical University Dresden. He received his diploma from the University of Hamburg (Institute for Laser Physics, 2008) and his Ph.D. from University of Freiburg (Institute of Microsystems Engineering, 2011). He then worked as a postdoctoral researcher at Georgia Tech, Atlanta, USA (School of Materials Science and Engineering, 2014) and University of Bayreuth (Institute of Physical Chemistry, 2015). Currently, his group focuses on understanding and exploiting the light–matter interaction of self-assembled plasmonic nanoparticles and quantum emitters to develop metasurfaces with unique optical properties.



**Andreas Fery** has been head of the Institute for Physical Chemistry/Polymer Physics at the Leibniz Institute of Polymer Research, Dresden and Professor for Physical Chemistry of Polymeric Materials at the Technical University Dresden since 2015. He earned his diploma from the University of Konstanz in 1996, his Ph.D. (2000) and habilitation (2006) from University Potsdam/Max Planck Institute for Colloids and Interfaces, Golm (MPIKG). He worked as a postdoctoral researcher at Institute Curie, Paris until 2001 and group leader at MPIKG from 2001 to 2006. In 2006, he became an associate professor and, in 2008, full professor in Physical Chemistry at University Bayreuth. His research focuses on colloids and interfaces, emphasizing colloidal interactions, micro/nano-mechanics, pattern formation, and plasmonics.

diameters of 20–80 nm in water ( $n = 1.33$ ) illustrate this effect (Figure 1a). We chose Mie theory, because it gives a nearly exact solution of the absorption and scattering properties of plasmonic particles while requiring only modest computational resources. Moreover, knowledge of the nearly exact extinction properties is an important reference for comparison with other models. The effective extinction cross-section is defined by the intensity of extinction cross-section divided by the cross-sectional area of the scattering nanoparticle. This definition holds for all of the calculations discussed in this progress report, and the effective extinction cross-section makes the optical responses from different types of metal nanoparticles comparable. (3) The optical responses can also be tuned, when

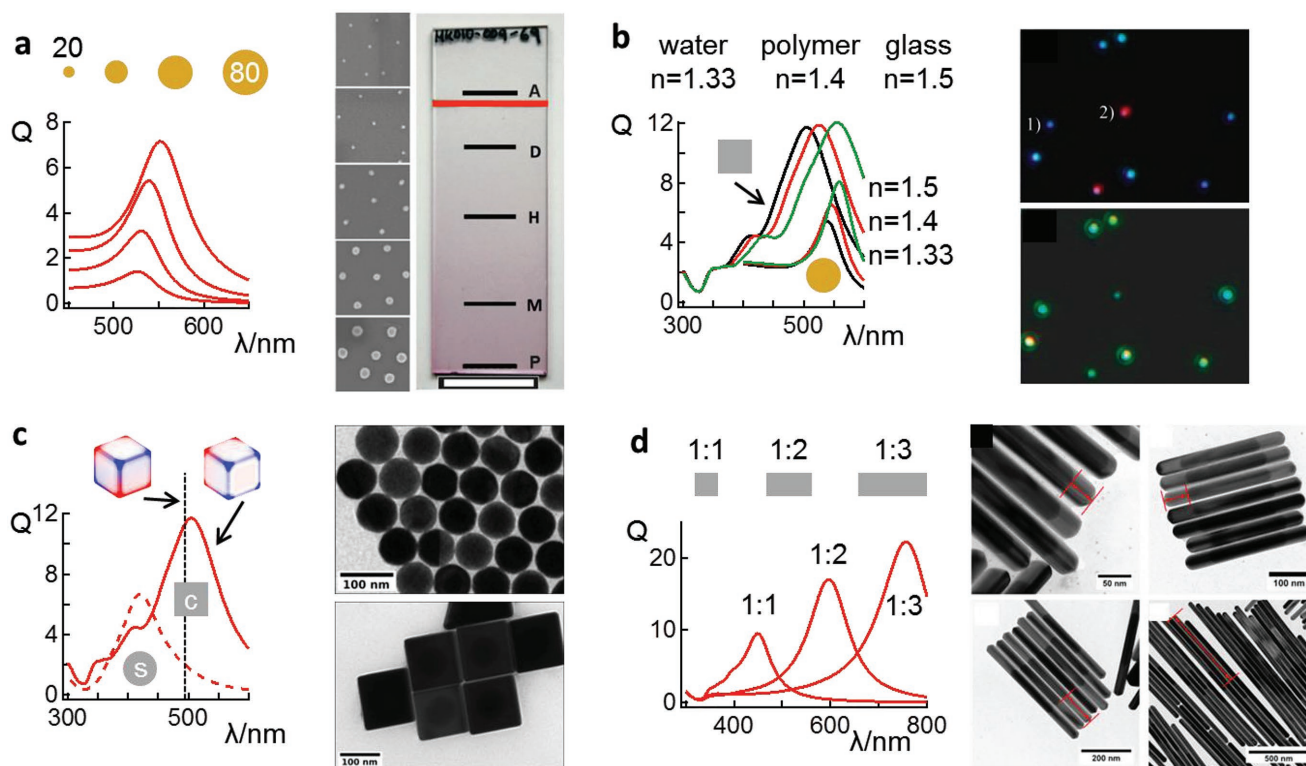


**Figure 1.** Design principles and colloidal plasmonic building blocks: Optical properties of colloidal building blocks shown by a) substrate-supported gradient plasmonic array of gold nanoparticles,<sup>[23]</sup> b) sensitivity to refractive index by dark field spectroscopy,<sup>[24]</sup> c) TEM image of spherical gold nanoparticles and silver shelled nanocubes,<sup>[22]</sup> and d) gold nanorods with tailored deposition of silver on the ends.<sup>[25]</sup> Definition of abbreviations: effective extinction cross-section ( $Q$ ), wavelength ( $\lambda$ ), sphere ('s') and cube ('c'). Electromagnetic modeling by Mie theory and FDTD method. (a) Adapted with permission.<sup>[23]</sup> Copyright 2014, American Chemical Society. (b) Adapted with permission.<sup>[24]</sup> Copyright 2003, American Chemical Society. (c) Adapted with permission.<sup>[22]</sup> Copyright 2017, Wiley-VCH. (d) Adapted with permission.<sup>[25]</sup> Copyright 2015, American Chemical Society.

the refractive index of the dielectric environment is systematically increased from water, to polymers, and to glass (Figure 1b). Increasing the refractive index of the surroundings results in an excitation at lower energy and an increase in effective extinction, which is caused by an increase in polarizability and lower damping, respectively.<sup>[26]</sup> All of the Mie theory calculations in this progress report can be reproduced by using the MATLAB (MathWorks) code implementation written by Mätzler.<sup>[27]</sup> In order to reproduce the calculations of the optical response at a particular wavelength, the complex refractive index constant must be reasonably approximated from fitting experimental data using polynomial functions. For the dielectric properties of gold, we utilized the sample data from Johnson and Christy,<sup>[28]</sup> which was fitted using sixth-order polynomial function with a root mean square (RMS) error of 0.2 over the range of 300–1600 nm. We chose the data of Johnson and Christy, because it shows the best match between simulated and experimental optical response. The optical constants of the environment (water, polymer, glass) were assumed to be constant for all wavelengths. If higher precision is necessary for optical constants of the environment, the online refractive index database is a useful resource.<sup>[29]</sup> The Mie theory can now be used as a tool to interpret spectroscopic data obtained for nanoparticles formed by wet-chemical synthesis. By comparing experimental spectra to Mie theory fits, the size and shape of the plasmonic nanoparticles can be determined. For instance, the presence of

anisotropy and facets would lead to a broadening and/or red-shift of the localized surface plasmon resonance, as discussed below.

Colloidal dispersions formed through wet-chemical synthesis methods are employed in a wide range of applications. Wet-chemical methods allow tuning of the optical response of plasmonic nanoparticles in a cost-efficient manner. Although methods for synthesizing simple gold colloids are already well established, utilizing these nanoparticles as building blocks for assemblies on plasmonic metasurfaces requires fulfillment of additional criteria:<sup>[30]</sup> Dispersity in size and shape lead to the broadening of the plasmonic peak extinction due to superposition of the optical response of all (different) nanoparticles in the ensemble. Modern synthesis, in some instances, however, can reach theoretical limits of optical quality for colloidal ensembles. For example, González-Rubio et al. impressively showed that the optical linewidth of gold nanorods can be reduced close to the theoretical limit by femtosecond laser reshaping.<sup>[31]</sup> Especially seed-mediated growth has proven to result in small size and shape variations meeting the requirements of high optical quality (Figure 1a).<sup>[32]</sup> In this synthesis approach, the nucleation of the particles known as the seeding and growth stages are separated from each other. Typically, such seeds (<5 nm diameter) are formed by a fast reduction with a strong reducing agent, followed by a slow and controlled overgrowth to achieve the final size and shape under milder conditions.<sup>[33]</sup> Since the

dispersity of the final particles is inherited from the initial seeds, this synthesis approach can yield particle size distributions with a standard deviation of the diameter well-below 5%.<sup>[34]</sup> Besides the size dispersion, the shape yield, i.e., the amount of morphological by-products of the synthesis also hinders assembly processes and gives in consistent optical properties that often appear as broadening of spectral features. This size and shape distributions can often be improved by additional purification steps, such as exploiting depletion forces.<sup>[35]</sup> Material is lost during each purification step, however, so a highly pure sample can be obtained from a polydisperse mixture only with low yield.

The introduction of nanoparticles with anisotropic shapes is an exciting development that extends the accessible range of excitation wavelengths and allows high sensitivity in comparison to spherical particles (Figure 1d).<sup>[36]</sup> Anisotropic shapes result in anisotropic surface plasmon resonances with more complex and tunable optical properties.<sup>[37]</sup> (4) The number of plasmon modes increases, when there are more different ways of polarizing the nanoparticles in respect to the electric field of light.<sup>[38]</sup> Figure 1d depicts nanorods, which can be excited by the electric field vector parallel (longitudinal mode) or perpendicular (transverse mode) to the long axis of the nanorod. Methods for synthesizing nanoparticles with anisotropic shapes or sharp edges and corners are well established.<sup>[39]</sup> In seed-mediated growth, the nanoparticle shape can be tuned through passivation and selective stabilization of specific crystal facets.<sup>[40]</sup> Most prominently, surfactants containing halides—or in the case of gold nanorods, combined with silver nitrate—act as shape-directing agents by energetically favoring growth of certain facets of the crystal.<sup>[41]</sup> Facet-selective growth gives rise to a variety of morphologies including spheres, triangles, cubes, and rods.<sup>[42]</sup>

It is also important to be able to control the faceting of nanoparticles, between the limits of spheres and cubes, which can be obtained through overgrowth processes or polyol processes.<sup>[43]</sup> The following design rules are determining the optical properties of spheres, cubes, and intermediate shapes of plasmonic nanoparticles (Figure 1c): (5) The plasmon shifts red, when fewer geometric symmetries are available and (6) multipolar modes can be excited. In addition to multipolar modes, an interesting feature of cubic structures is the possibility to excite bright and dark modes. (7) Due to their typical signature of surface charge oscillation at the metal–dielectric interface, plasmonic nanoparticles can be approximated as dipole oscillations. This dipole can couple to light and is defined as bright mode. (8) On the other hand, when quadrupole mode is excited (dipole moment is zero), the mode is defined as dark mode, where no direct coupling to light is possible.<sup>[44]</sup>

For electromagnetic simulations of nonspherical nanoparticles shown above (Figure 1), we used a commercial-grade simulator based on the finite-difference time-domain (FDTD) method (Lumerical FDTD).<sup>[45]</sup> For investigating the scattering behavior of the plasmonic nanoparticles, a source designed for scattering behavior of objects (total-field scattered-field source) was utilized to isolate the scattering field from the incident field. A balance between the computational effort and accuracy, which can be validated by comparison with Mie theory calculations, is a consideration when using this finite-element method. Thus, we have set the frequency points to be half the wavelength span and the

mesh size to 1 nm. For objects smaller than 20 nm, even smaller mesh sizes are necessary. Finally, the injected electromagnetic field must converge during the defined simulation time. For the dielectric properties of silver, a CRC Handbook of Chemistry and Physics approximation by Hagemann et al. was used (five coefficient, 0.2 RMS error, 300–1200 nm fitting range).<sup>[46]</sup> In order to calculate the surface charges of the bright and dark modes in Figure 1c, we have implemented the electrostatic limit approximation from Zhang et al.<sup>[44]</sup> into FDTD. Briefly, this approximation considers in its calculations small object sizes (3 nm), symmetric/antisymmetric boundary conditions and optical constants from the Drude model (intradband only).

Similar results can be achieved using noncommercial solutions, which is appealing for researchers who may use plasmonic nanoparticles in their research but do not specialize in optical property simulations. For example, the discrete dipole approximation (DDA) method can calculate extinction responses for particles of arbitrary shape. The open source code implementation by Draine and Flatau (DDSCAT) and by nanoHUB (nanoDDSCAT) is widely used.<sup>[47]</sup> However, the DDA method has a significant disadvantage in computational effort when surfaces are added, since these surfaces must be approximated also by dipoles.

To be complete, we briefly discuss various simulation methods to determine the optical response of structured multilayer stack: Multilayer planar stacks can be calculated by the analytic transfer matrix method.<sup>[48]</sup> The complex reflection and transmission coefficients can be calculated either using custom code, publicly available programs for FDTD (stackrt and stackfield), or other commercial solutions. For simulating periodic structures, a semianalytical method such as rigorous coupled-wave analysis is recommended.<sup>[49]</sup> Analytical and semianalytical methods can contribute to a better understanding of optics because of their computation efficiency in comparison with numerical methods, as discussed in the review article by García de Abajo and co-workers.<sup>[50]</sup>

## 2.2. Plasmonic Excitation across the Entire Visible Spectrum: From Gold to Silver

The optical and chemical properties vary widely among plasmonic materials. In this section, we compare the optical properties and wet-chemical syntheses for the most commonly used plasmonic materials. For plasmonic excitation in the visible spectrum (380–750 nm), silver is generally the preferred material for colloids rather than gold. The reason lies in the quality factor (QF), which was introduced by Wang and Shen and defined,<sup>[52]</sup>  $QF = \frac{\omega(d\epsilon'/d\omega)}{2\epsilon''}$ , where  $\epsilon'$  and  $\epsilon''$  are the real and imaginary parts of the dielectric function ( $\epsilon$ ) of the metal, respectively. Thus, a large QF is obtained when  $\epsilon''$  is small and the change in  $\epsilon'$  is large. As shown in Figure 2a, silver has a large QF in the blue, and has a significant QF across the entire visible spectrum, while gold's QF vanishes in the blue. The observed effect is also correlated with the band transition from intraband to interband of silver (at 326 nm) and gold (at 515 nm).<sup>[46]</sup> Because of the distinct optical properties of silver and gold, the expected dipolar resonances for silver

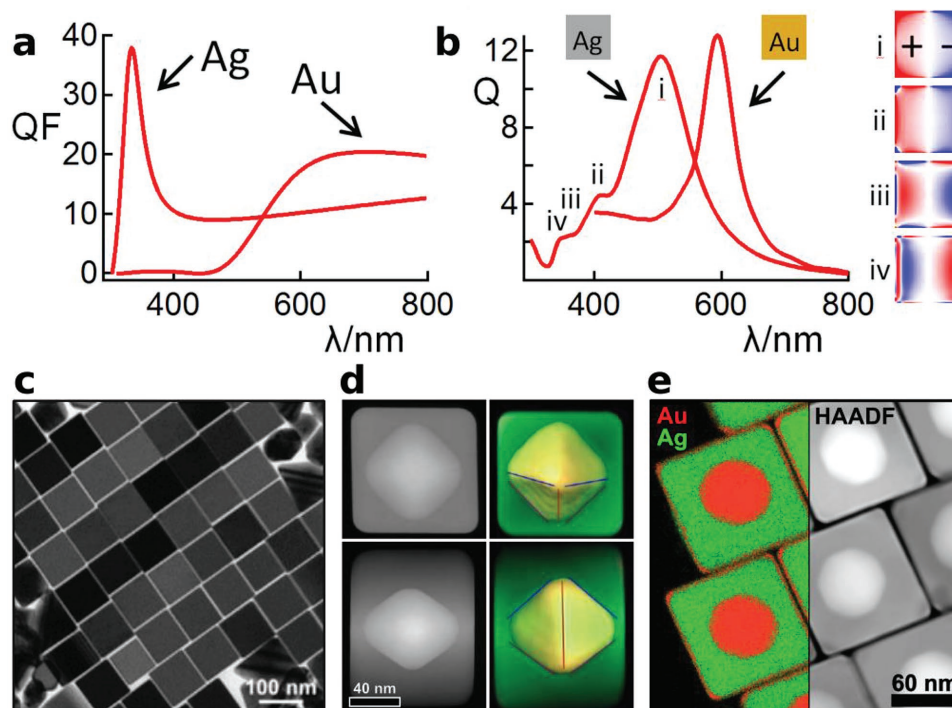


**Figure 2.** Plasmonic quality factor and examples of well-defined and stable silver nanoparticles: a) Wavelength-dependent quality factor (QF) for bulk silver and gold in the visible spectrum. b) Spectroscopic response of 60 nm silver and gold cubic nanoparticle in water and surface charge images of the silver plasmonic modes from FDTD calculations. c) Finely-tuned surfactant-based silver nanocube synthesis as shown by Xia and co-workers. Alternatively, d) silver overgrowth from gold particle seeds inheriting their size distribution and crystal structure. The abbreviations are defined as follows: effective extinction cross-section ( $Q$ ) and wavelength ( $\lambda$ ). e) Subskin-depth gold layer as oxidation protection for silver nanoparticles. (c,d) Adapted with permission.<sup>[43a,51]</sup> Copyright 2016/2013, American Chemical Society. (e) Adapted with permission.<sup>[22]</sup> Copyright 2017, Wiley-VCH.

and gold nanocubes occur at 505 and 595 nm, respectively. It should be noted that the energetically lowest modes for silver and gold are both dipolar. For clarity in Figure 2b, the plasmonic dipolar mode was only labeled and illustrated for silver. Due to the high QF of silver in the ultraviolet range, energetically higher plasmonic modes can be observed as well. These higher plasmonic modes are potentially useful for propagating energy because of their lower radiative damping.

The sensitivity of silver to oxidation makes the synthesis of durable silver nanoparticles challenging and poses some experimental limitations. Gold, in contrast, is the most noble metal and is least prone to oxidize upon contact with ligands or the environment. Furthermore, the size and shape of gold nanoparticles can be readily controlled following a vast range of well-established synthetic protocols.<sup>[39]</sup> Consequently, gold nanoparticles are commonly the material of choice for proof-of-concept realizations of plasmonic metasurfaces.<sup>[53]</sup> Despite the superior optical properties of silver, the number of reproducible and tunable protocols that result in a narrow distribution of nanoparticles as well as high yield of shaped nanoparticles is limited.<sup>[51]</sup> These protocols typically involve chemical-passivation of the particle-surface by polymer layers like polyvinylpyrrolidone (PVP).<sup>[25,51]</sup> The drawback of passivation by a polymeric layer can be overcome through recent advances in surfactant-based synthesis<sup>[51]</sup> and/or the use of well-defined gold particles as seeds for the silver deposition.<sup>[25,43a,54]</sup> depicted in Figure 2c–e. In the later approach, the narrow size

distribution of the gold cores is templated into highly uniform silver shell, which dominates the optical properties by masking the gold core. By combining the superior optical properties of silver and the synthetic advantages of gold in this manner, wires, cubes and cuboidal morphologies with outstanding optical properties can be achieved.<sup>[22,25,43a]</sup> Recent developments have also established silver nanocubes that are stable against oxidation, while keeping the surface functional, by overgrowth of a protecting gold layer with a subskin depth thickness (i.e.,  $\approx 1$  nm), as shown in Figure 2e.<sup>[22]</sup> This method allows for the combination of the colloidal and synthetic stability of gold with the high optical quality of silver, because the effect of the thin gold shell is negligible.

### 2.3. Short- and Long-Range Coupling in Colloidal Plasmonic Metasurfaces

With the optical properties of noninteracting nanoparticles and methods for synthesizing and engineering the optical properties of plasmonic nanoparticles established, this section is dedicated to understanding the properties of nanoparticles on surfaces with broken symmetry, including short- and long-range coupling effects between the nanoparticles. The plasmonic hybridization that occurs through symmetry breaking is important for understanding the properties of plasmonic metasurfaces.

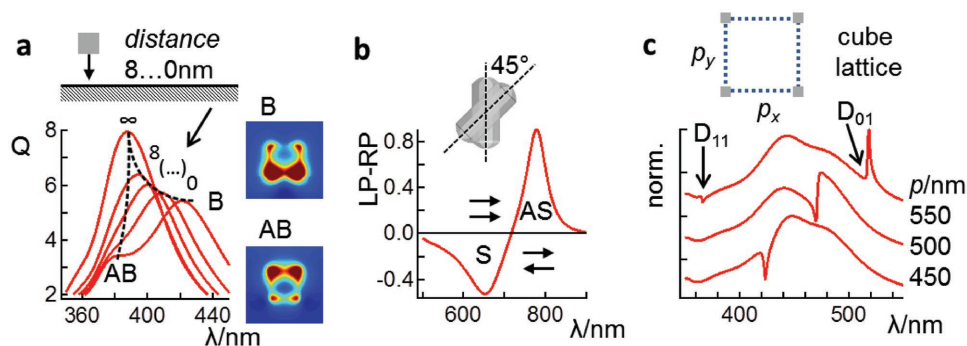


**Figure 3.** Design principles for breaking the symmetry of plasmonic nanoparticles: Simulations of plasmonic hybridization a) when a silver cube approaches a dielectric substrate (bonding and antibonding (B/AB) modes), b) for twisted dimers of silver nanorods (symmetric and antisymmetric (S/AS) modes), and c) first-order Bragg diffraction ( $D_{01}$ ) in a periodic lattice. All effective extinction cross-sections ( $Q$ ) are calculated in water ( $n = 1.33$ ), except for (a) symmetry breaking with a substrate ( $n = 1.5$ ) and air ( $n = 1$ ) in the gap. The abbreviations are defined as follows: wavelength ( $\lambda$ ), left and right polarized (LP/RP, respectively) light, and lattice periodicity ( $p$ ). Electromagnetic modeling by FDTD method.

Since the symmetry of the dielectric environment is broken by placing a plasmonic nanoparticle onto a substrate, it has a pronounced impact on the spectroscopic properties of the system (Figure 3a). Another type of complexity arises when plasmonic nanoparticles interact, such as stacked nanorods (Figure 3b) or an arrangement in periodic lattices (Figure 3c). In each of these examples, two or more plasmon resonances overlap and interact with each other. These interactions result in an asymmetric line-shape (Fano resonance), where the extinction of the coupled resonators has a distinct minimum and maximum arising from the coupling. Because of the wide range of simple interactions that give Fano resonances, Fano line shapes are commonly observed in many plasmonic systems. The sharpness of the Fano resonance makes it highly appealing for several applications. For example, structural color can be brighter than pigmentary colors, is immune to photo bleaching, and can be tuned dynamically, if the system is mounted on a flexible substrate.<sup>[55]</sup> Nonlinear effects, such as lasing, can be achieved when light is coherently coupled to a periodic nanostructure.<sup>[56]</sup> Further applications include highly sensitive refractive index sensors<sup>[57]</sup> and selective injection of hot electrons.<sup>[58]</sup> For further reading about Fano resonances at plasmonic metasurfaces, we recommend the review from Chong and co-workers.<sup>[59]</sup> In an analogy to classical coupled oscillators, the Fano resonance usually occurs when broadband resonance interacts with a narrowband resonance.<sup>[60]</sup> In the case of a nanocube on a substrate, the interaction between the bright mode (broadband) and dark mode (narrowband) is responsible for the asymmetric line shape (see also bright and dark mode in Figure 1c). As shown in Figure 3a, the interaction results in a lower-energy bonding mode and higher-energy antibonding mode. The antibonding mode is useful for applications in sensing because of enhanced electric field facing toward the environment.<sup>[61]</sup> Plasmonic field enhancement from the gap between the nanoparticle and substrate (nanocavity) is important for plasmon-induced hot electron injection<sup>[62]</sup> controlling radiative processes in such plasmonic cavities.<sup>[63]</sup> A limiting factor in colloid-based approaches is the presence of stabilizing surfactants ( $\approx 2$  nm thickness) around the nanoparticle, which can limit charge transfer and the gap size. Despite the possibility of removing this dielectric shell by plasma cleaning or

heat or chemical treatment,<sup>[64]</sup> it is usually preferable to functionalize the particles with adequate alternative ligands (see also Section 3.1).

The Fano resonance can be described in analogy to the hybridization model of molecular orbital theory, where the resulting plasmonic modes can be described as the linear combination of resonances of the two isolated modes.<sup>[65]</sup> Twisted nanorods dimers demonstrate this concept, where the dipole modes of each nanorod hybridize into symmetric and antisymmetric modes.<sup>[66]</sup> The optical responses of chiral plasmonic systems can be evaluated by calculating the difference between left and right polarized light in extinction (Figure 3b). The negative sign corresponds to the symmetric mode, while the zero crossing corresponds to the primary plasmonic mode (the longitudinal mode of an isolated nanorod) and the positive sign corresponds to the antisymmetric mode. The same optical signature can also be observed for the hybridized transverse mode (not shown). It is important to note that the symmetric and antisymmetric plasmon modes are connected to the electric permittivity and magnetic permeability, thereby making such chiral systems attractive for applications in negative refractive index materials.<sup>[66]</sup>

Another approach for generating a narrow and asymmetric line shape is by diffractive coupling of the localized plasmon mode with a Bragg grating, also known as surface lattice resonance (Figure 3c), which is special type of Fano resonance. The wavelength location of the first Bragg mode ( $D_{01}$ ) is proportional to the lattice constant  $a$  and the refractive index  $n$  of the surrounding media ( $D_{01} \propto n \times a$ ),<sup>[67]</sup> which results in tunability of the surface lattice resonance by changing the periodicity. Recently, Gérard and co-workers identified the resulting hybridized lattice modes as delocalized “photonic-like” (energetically lower resonance) and localized “plasmonic-like” (energetically higher resonance) modes.<sup>[68]</sup> For simulating surface lattice resonances by FDTD, the previous selected boundary condition (in the lattice plane only) must be changed from a perfect matched layer to periodic boundary conditions. The same optical response can also be attained by using inverse structures, such as nanohole arrays, which is known as Babinet’s principle.<sup>[69]</sup> The tunability of surface lattice resonances makes them attractive for structural color<sup>[56]</sup> or for strong coupling to obtain lasing, when the system is coupled to an emitter.<sup>[70]</sup>

### 3. Principles of Colloidal Self-Assembly

Self-assembly is the spontaneous organization of pre-existing components into complex organized structures.<sup>[71]</sup> Self-assembly is controlled by the chemical and physical properties of nanoparticles, surfaces, and their interactions.<sup>[6]</sup> The driving force for the organization of these structures is the reduction of free energy to approach local equilibrium. Approach a specific local equilibrium can be externally aided or modulated by exploiting directing fields and/or confinement effects. In the directed self-assembly processes, templates, external fields, or directing agents are typically used to induce selective clustering of colloids and spatial order. For template-assisted colloidal self-assembly—the primary method for bottom-up fabrication of colloidal metasurfaces—capillarity and capillary forces drive self-assembly process on the interface of templates (i.e., surface-modified objects with selective binding sites).

Recent developments in colloidal science have enabled the precise self-assembly of plasmonic nanoparticle, resulting in well-controlled emergent properties through plasmon coupling. In particular, simultaneous progress in surface modification, miniaturization of features, and improved scalability of template fabrication in the last decade have led to significant advances in self-assembly.<sup>[4b,72]</sup> The improved reproducibility and fine control now available through templated self-assembly provide a strong and necessary foundation for complex spatial organization that is required for applications. The field of template-assisted self-assembly has matured to a point, where efficient scalability, how to obtain precise control, and subsequent system integration need to be considered early in the development of self-assembly processes.

Following the theory of plasmon hybridization, complex materials can be constructed from their primary components by stepwise introduction of additional nanoparticles to a plasmonic metasurface, increasing its size. As visualized in **Figure 4**, for large, periodic assemblies obtained in this manner, long-range lattice effects can dominate the properties. Hence, hierarchical plasmonic metasurfaces can be designed by assembling the colloidal building blocks in a rational manner.<sup>[73]</sup>

(I) As represented by nanospheres, nanocubes, and nanorods in Figure 4Ia, colloidal (noble metal) nanoparticles constitute the primary component. The optical properties are defined by the composition and shape of the nanoparticles, as discussed in previous sections. The resulting metasurfaces from a stepwise increased number of interacting particles in the unit cell can be grouped as follows:

- (II) A group consisting of a few building blocks support additional properties such as Fano resonances and/or electric/magnetic resonances. Therefore, they are dominated by the local coupling, which is dependent on the coupling strength and the number of particles. The most basic motif is a closely coupled particle dimer (IIb), which can be further simplified to a single particle coupled to a dielectric or metal surface that breaks its symmetry (IIa), as illustrated in Figure 4 (group II).
- (III) For linear particle chains or plasmonic polymers, the optical response is independent of the number of particles in the chain due to the radiative damping—thereby distinguishing them from smaller clusters.<sup>[74]</sup> Linear particle chains are particularly interesting for subwavelength energy and information transport applications or applications in strain sensing, as a result of their directional and anisotropic optical properties.<sup>[74a,75]</sup>
- (IV) In the case of plasmonic crystals, the building blocks are arranged in a period array to exploit the collective coupling effects induced by the long-range ordering of well-separated nanoparticles. The resulting Fano resonances are sharp because they combine coherent coupling of the individual plasmon modes and Bragg diffraction of the lattices.

(Ia) Role of surface functionalization of individual nanoparticles

For achieving well-controlled colloidal self-assembly, several requirements of the building blocks and the templates need to be met. Hence, the surface properties of the colloids, defined by their chemical functionalization, are essential for the self-assembly process and need to be matched to the chosen assembly technique. The main requirements are (1) colloidal stability in solution, (2) suitable properties of the spacer material between adjacent building blocks, and (3) the ability to form connections between the template and the directing fields and/or confinement effects during the assembly process. These features are determined by the (typically organic) ligand stabilizing the nanoparticles, which is either employed as the capping agent when synthesizing the nanoparticles or can be modified or exchanged later via functionalization or ligand exchange in an additional step. Several examples of functionalization for assembly are summarized in **Table 1**.

- (1) The colloidal stability of nanoparticles is especially important during the self-assembly process: the ligand has to prevent irreversible agglomeration, even in situations when external forces acting during the assembly process bring the nanoparticles into contact with each other.<sup>[76]</sup> Colloidal stability needs to be attained at high concentrations in order to prevent

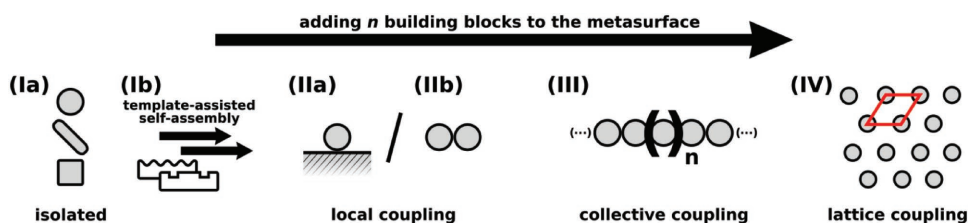


**Figure 4.** Self-assembly concepts for colloidal metasurfaces via incremental increase in the number of particles in the unit cell: (I) Colloidal particles with well-defined morphology (Ia) and templates (Ib) as building blocks for the self-assembly; (II) unit cells from (IIa) surface-coupled colloids or (IIb) few closely placed colloids, both dominated by near-field coupling; (III) 1D plasmonic “polymers” from spheres acting as quasifinite chains by collective coupling within the particle cluster; and (IV) 2D lattices with long-distance order resulting in surface lattice plasmons.

**Table 1.** Surface functionalization of nanoparticles for self-assembly.

Cat.	Purpose	Type of functionalization	Example	Thickness	Ref.
(1)	Capping agent	Surfactant from synthesis	CTAB, CTAC	<5 nm	[41]
(1)	Capping agent	Polymer from synthesis	PVP/polyol	<5 nm	[25,51]
(2)	Responsive Spacer	Responsive polymer/hydrogel	PNIPAm, PVP-Gel	<1 μm	[78,79b,80b]
(2)	Spacer	Inorganic (+label)	SiO <sub>2</sub>	>5 nm	[63c,83]
(2)	Conductive spacer	Conductive polymer	PEDOT:PSS, PANI	<50 nm	[79a,80c]
(2)	Responsive spacer	(Labeled) protein/DNA	BSA, DNA	<10 nm	[77a,79d]
(3)	Wetting modification	Surfactant for assembly	SDS/Triton	–	[76]
(3)	Hydrophobic linking	Polymer for assembly	PSS/P2VP	<5 nm	[82a]
	Electrostatic linking		PAH/PVP	<5 nm	[84]
	Wetting modification		PEG-SH	<2 nm	[85]
(3)	Chemical linking	DNA	ssDNA, DNA	≈1 nm	[86]

uncontrolled agglomeration. The assembly process can be accompanied by changes in ionic strength and pH. Thus, the nanoparticles need to be stable over a range of pH and ionic strength. This can be achieved by electrostatic or steric (or both combined: electrosteric) interactions.<sup>[77]</sup> Typically, colloidal stability is provided by the capping-agent used in the synthesis, e.g., cetyltrimethylammonium bromide (CTAB) or PVP. Unfortunately, these ligands often lack functionality and/or are incompatible with assembly processes. Replacing the initial capping-agent via functionalization with polymeric ligands can introduce the required properties/functionality, for example the inversion of surface charges.

- (2) Beyond providing colloidal stability, ligands can act as a dielectric spacer in the plasmonic metasurface and introduce tunability and responsiveness, thereby enabling and affecting the optical properties of the metasurface.<sup>[78]</sup> Synergistic effects between colloids and spacers or substrates can be introduced via “smart” ligands. A few examples include (semi-)conducting polymers, poly(*N*-isopropylacrylamide) (PNIPAm) as temperature responsive polymer, or fluorescently labeled DNA/protein.<sup>[79]</sup> By employing smart ligand, properties such as conductivity, environmental responsiveness, (e.g., pH or temperature), and optical effects like fluorescence can be introduced into the system.<sup>[80]</sup>
- (3) Most of the different self-assembly processes, which are discussed later, require optimizing interactions between the colloidal nanoparticles and the surface, as well as wetting of the colloidal dispersion. Surface modification of the nanoparticles can be used to render both their interactions and wetting behavior compatible with the assembly process. Examples for tuning wettability can be found in refs. [76] and [81] and ref. [78]. As explained in refs. [76] and [81], the contact angle of the wetting solution defines the strength of the capillarity, which is exploited for the assembly process. In ref. [78] the colloids are rendered surface active by a polymeric shell, in order to freely float on the water–air interface. Examples for the significance of particle–surface interactions can be found in ref. [82]. In these examples assembly on the templates is achieved via hydrophobic–hydrophobic interactions,<sup>[82a]</sup> electrostatic interactions,<sup>[82b,c]</sup> and chemical linking.<sup>[82d]</sup> Surface functionalization guides

the interactions with the template, which can include complementary charges or highly selective groups, such as DNA.

#### (Ib) Role of the template

The role of the template is to direct the forces guiding self-assembly to produce hierarchically ordered nanoparticle assemblies.<sup>[72b]</sup> Templates have specific binding sites for the approaching colloids, which employ chemical linkers to form bonds or attractive interactions, spacers that provide repulsive interactions, or topographical traps. Templates are often designed to engineer specific interactions with nanoparticles, based on the size, shape, and chemistry of the nanoparticles. An overview of templates that have already been employed for template-assisted self-assembly is provided in the next section. The examples are sorted from those giving high positional control for the assembly to those that are scalable and cost efficient—which is the general sorting scheme in this progress report. These selected examples were chosen for the outstanding and/or recent results of assembled nanoparticles without respect to the novelty of the method for fabricating the template.

For chemically structured templates (**Figure 5a,b**, top line), sub-micrometer-sized chemical contrast is crucial for providing attractive and repulsive regions for physis- or chemisorption. Exploiting the dielectric shell encapsulating the colloids as spacer is commonly employed for obtaining ordered (mono) layers. The shell serves as a template for close-packed films, allowing tuning of the interparticle distance via the shell thickness and its hydrophobicity.<sup>[23,77b,78,90]</sup>

Chemically structured templates can be fabricated by nano/microcontact printing. In this process, chemical contrast is printed using a topographic stamp by transferring/removing binding sites onto/from a target surface. The resolution of the template primarily depends on the resolution of the stamp, and a several different types of chemical contrast are commonly used, including charge, hydrophobicity, and reactive linking groups.<sup>[82a,91]</sup>

Microphase separation can also be used to provide contrast on templates. A common method is tailoring and fabricating block-copolymers with contrast embedded in the different blocks.<sup>[92]</sup> However, controlled formation of grains and domains

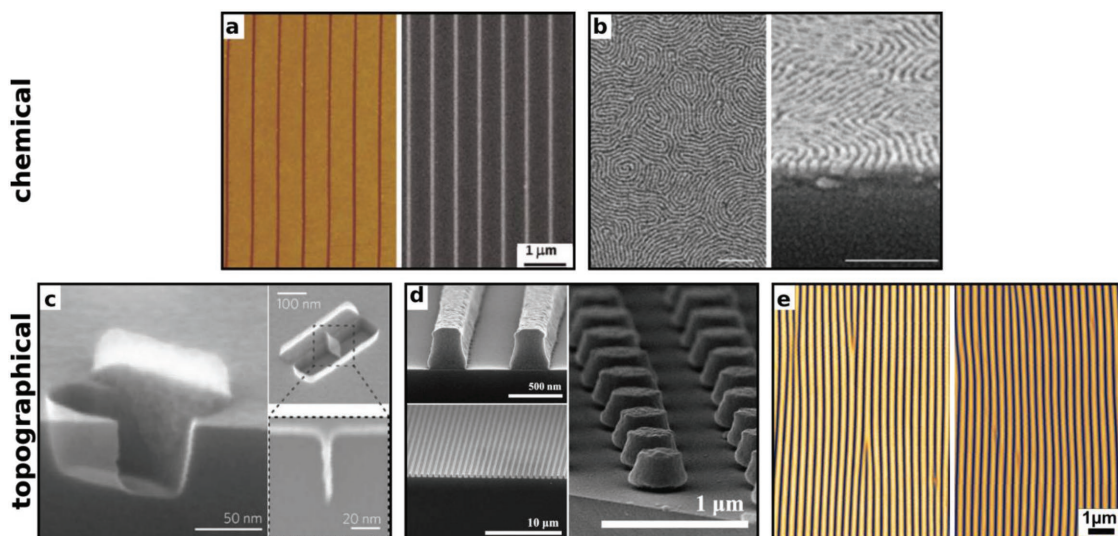


**Figure 5.** Chemical (top) or topographical (bottom) templates for colloidal self-assembly: a) Microcontact printing ( $\mu$ CP) to stamp chemical contrast onto a target: polyelectrolytes. b) Microphase separation of block-polymers featuring chemical contrast (scale bars: 100 nm). c) Topographic traps fabricated via high-resolution electron beam lithography. d) Laser interference lithography to form channels and more complex structures. e) Periodically wrinkled templates formed by mechanical instabilities due to modulus mismatch between an elastomer slab and its surface layer. (a) Adapted with permission.<sup>[82a]</sup> Copyright 2012, American Chemical Society. (b) Adapted with permission.<sup>[87]</sup> Copyright 2017, American Chemical Society. (c) Adapted with permission.<sup>[36a]</sup> Copyright 2016, Springer Nature. (d) Adapted with permission.<sup>[88]</sup> Copyright 2011, Elsevier. (e) Adapted under the terms of CC-BY license.<sup>[89]</sup> Copyright 2015, Royal Society of Chemistry.

needs to be considered for the scalability of this approach. By selective etching of one component of the microphase, the chemical template can also be converted into topographical structures, thus bridging chemical and topographical template approaches.<sup>[93]</sup>

Topographical templates (Figure 5c–e) can provide excellent control over the self-assembly process, resulting in highly ordered structures by providing local energy minima. The selectivity of topographical templates is determined by the geometry of the features and their dimensions.<sup>[36a,b,81,91]</sup> Templates fabricated via electron beam lithography or focused ion beam milling have the highest degree of control and versatile trap geometries. This flexibility to create arbitrary template structures comes at a relatively high cost, however, and generally lacks efficient scalability to macroscopic areas. Therefore, these kinds of templates are only well suited for the proof-of-concept plasmonic metasurfaces. Laser interference lithography is a scalable alternative to these methods, whose resolution is limited by the diffraction limit of light. Topography is constructed by interference of multiple laser beams at a photoresist, utilizing the phase of light. The types of patterns that can be fabricated by interference lithography range from periodic lines and elliptical holes to holes/pillars in hexagonal or square lattices.

Arrays of periodic lines can be fabricated in an extraordinarily inexpensive and scalable manner, as compared to conventional lithographic methods. Centimeter-scale wrinkled structures can be formed through mechanical instabilities in polymer films, as explained in detail in the reviews and book chapters by Schweikart et al.<sup>[92]</sup> For example, periodicities down to 200 nm can be fabricated by simply stretching a flat slab of an elastomer, polydimethylsiloxane (PDMS), followed by introducing elastic modulus mismatch by plasma hardening of

the surface layer and subsequent relaxation of the PDMS.<sup>[89,95]</sup> The wrinkled structures that result (Figure 5f) are well suited as templates for colloidal self-assembly of nanoparticles into macroscopic plasmonic metasurfaces. In summary, several different methods are available for template self-assembly of plasmonic nanoparticles, and the precision of the assembly, scalability, and cost are key considerations.

#### (IIa) Building plasmonic metasurfaces from single nanoparticle assemblies on substrates

One limiting behavior of plasmonic metasurfaces is individual clusters that do not rely on interactions between neighboring unit cells, but obtain their optical properties by local coupling (depicted schematically in Figure 4IIa,b). The only plasmonic coupling is within clusters of nanoparticle particles, e.g., dimers deposited from solution or formed during deposition, or coupling to a dielectric/metallic substrate, which enhances its electromagnetic field.

Formation of particle assemblies on surfaces will typically use the surface as an element in guiding the assembly process, in contrast to bulk solution fabrication, which is not discussed here. One of the most basic concepts is coupling a single plasmonic nanoparticle with a surface, either a dielectric surface to induce symmetry breaking,<sup>[44,97]</sup> or a metal film to induce plasmon coupling with the induced image charges.<sup>[98]</sup> Nanoparticles can be deposited on substrates through many common techniques, such as drop-casting,<sup>[99]</sup> spin-coating,<sup>[23,98c]</sup> and Langmuir–Schaefer techniques.<sup>[78,100]</sup> Hybridized plasmon modes,<sup>[44]</sup> magnetic resonances,<sup>[101]</sup> and high sensitivity can result from the formation of plasmonic cavities.<sup>[101,102]</sup> A key feature of such systems is the high sensitivity and tunability of the plasmonic response by varying the distance between the nanoparticle and the substrate. One

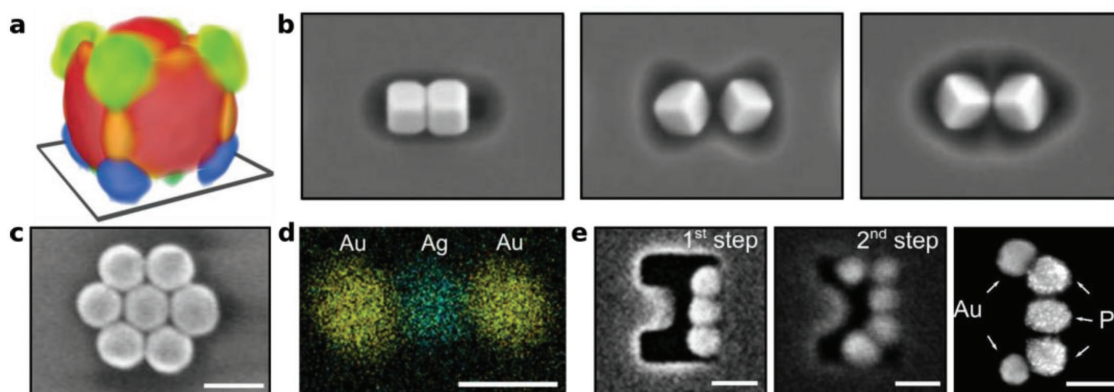


**Figure 6.** Plasmonic metasurfaces dominated by local coupling within plasmonically isolated unit cells. a) Plasmonic modes of an isolated nanoparticle coupled to a substrate, a simple and common design motif. b) Coupling scenarios for nanocube dimers. c) Circular heptamer supporting a hybridized plasmonic mode (scale bar: 200 nm). d) Heterotrimer consisting of two terminal gold particles and a central silver colloid (scale bar: 100 nm). e) Multimetallic U-shaped pentamer consisting of gold and platinum particles via successive assembly steps (scale bar: 100 nm). (a) Adapted with permission.<sup>[96]</sup> Copyright 2013, Springer Nature. (b) Adapted with permission.<sup>[36a]</sup> Copyright 2016, Springer Nature. (c) Adapted with permission.<sup>[74c]</sup> Copyright 2013, American Chemical Society. (d–e) Adapted with permission.<sup>[76]</sup> Copyright 2018, Royal Society of Chemistry.

of the most common structures is the coupling of a nanocube to a substrate (Figure 4IIa and Figure 6a),<sup>[96]</sup> which does not require fabrication of lateral features in the templates. The quality and smoothness of the substrate is important, however, for reproducible coupling, and the dielectric spacer can be exploited to introduce responsiveness to external triggers.<sup>[80,103]</sup> A recent example is the tuning of the distance between a gold nanoparticle and gold mirror by a thermoresponsive PNIPAm shell.<sup>[80b]</sup>

#### (IIb) Plasmonic metasurfaces from finite colloidal assemblies

Moving beyond substrate effects, interparticle coupling also has an important role in the formation of plasmonic metasurfaces (Figure 4III,IV). Thereby, the template provides steric hindrance for selective linking reactions resulting in anisotropic and more selective coupling scenarios. For example, plasmonic necklaces and dimer formations are feasible, as shown by Bach and co-workers and Yoon and co-workers, respectively.<sup>[104]</sup>

Capillarity-assisted particle assembly (CAPA) is a technique that provides precise positional ordering of the building blocks,

even for complex designs.<sup>[74c,105]</sup> The required topographic template imposes limits on the design, resolution, and the scalability of CAPA. Electron beam lithography is the predominant substrate fabrication method for CAPA because of its high precision and well established protocols.<sup>[36a]</sup> Self-assembly is triggered by pulling a meniscus of the colloidal dispersion droplet by a doctor-blade-like setup across the template (see Figure 7a). Nanoparticles are concentrated in the accumulation zone of the meniscus via convective flow. The concentration in the accumulation zone is controlled by the rate of evaporation of the meniscus front. The topographic features of the template define minima of the free energy and selectively trap the particles.<sup>[76,106]</sup> For CAPA the choice of stabilizing ligand is largely irrelevant, since trapping is triggered by capillary forces. Controlling the contact-angle of the moving meniscus, however, is critically important for directing capillary forces, while maintaining colloidal stability in the accumulation zone. The contact angle can be set by adding surfactants, which are typically also used as stabilizing ligands or need to be compatible with the ligands already on the nanoparticles.<sup>[76]</sup> CTAB—also in combination with cosurfactants—is sufficient for stabilizing the

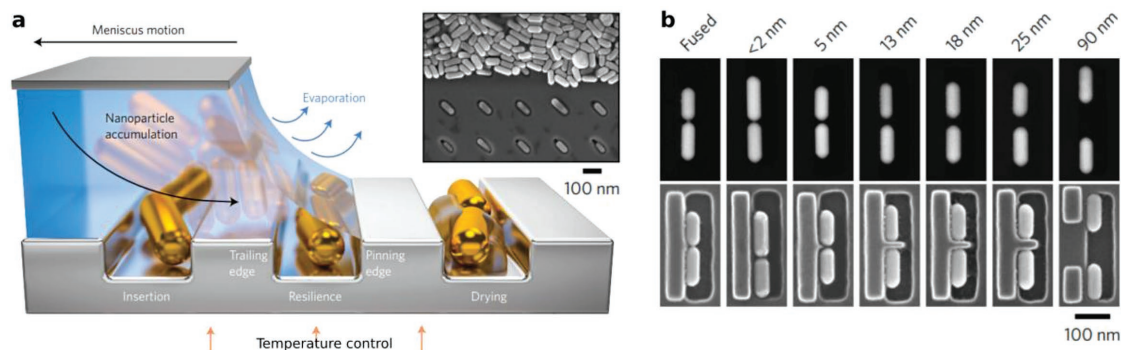


**Figure 7.** Capillarity-assisted particle assembly (CAPA). a) Assembly is triggered by pulling a colloidal dispersion over a topographic template. Nanoparticle accumulation is triggered by the evaporation process, resulting in nearly complete filling with nanorods. (Inset) Assembled nanorods and freeze-dried meniscus shows the high particle concentration in the accumulation zone. b) Electron beam lithography proves highly precise manufacturing of dimers. Adapted with permission.<sup>[36a]</sup> Copyright 2016, Springer Nature.

colloids.<sup>[76]</sup> Tuning the forces by controlling the contact angle and trap geometry allows trapping of single nanoparticles and successive assembly (sCAPA) of different types of nanoparticles, giving rise to complex multimetallic plasmonic clusters, shown by Ni et al.<sup>[76]</sup> Such multimetallic clusters hold great potential for several applications, such as charge and information transfer processes.<sup>[107]</sup> Selected examples of (s)CAPA are shown in Figure 6b–f, and many more details about this method can be found in the recent review article by Wolf and co-workers:<sup>[76]</sup> (b) simple dimeric nanorod antennas with tunable distance,<sup>[36a]</sup> (c) corner-connected nanocubes,<sup>[36a]</sup> (d) circular heptamers,<sup>[74c]</sup> and (e) multimetallic U-shaped assemblies.<sup>[76]</sup>

### (III) Regularly spaced nanoparticle chains

Plasmonic polymers are closely related to smaller clusters of plasmon-coupled nanoparticles. The transition between those two types of nanoparticle clusters is rather smooth (Figure 4). To define this term more precisely, we follow the definition of polymers by International Union of Pure and Applied Chemistry (IUPAC): A molecule can be regarded as polymer “(...) if the addition or removal of one or a few of repeat units has a negligible effect on the molecular properties.”<sup>[108]</sup> By analogy, we define plasmonic polymers via the sensitivity of their optical properties to the number of constituting nanoparticles. If the dominating plasmonic resonance (the super-radiant mode) does not change upon addition (or removal) of one or a few nanoparticles to the chain, such a linear colloidal cluster is a plasmonic polymer.<sup>[109]</sup> The critical number, above which a particle chain is a plasmonic polymer, is commonly referred to the infinite chain limit.<sup>[109]</sup> For linear chain-like plasmonic polymers, this threshold of repeat units is typically reached within

8–10 particles.<sup>[74b,110]</sup> Below the infinite chain limit, (linear) clusters are referred to plasmonic oligomers.<sup>[74a]</sup> The nature of the plasmonic modes in a linear assembly can be considered in analogy to the particle-in-a-box model from quantum mechanics. In this model, the end of the chain defines the potential barrier, and the plasmonic chain modes correspond to the energy eigenstates.<sup>[111]</sup> Results from classical electromagnetic simulations using coupled-dipole approximation methods can be used to get a qualitative understanding of these modes.<sup>[112]</sup> Quantitative results can be obtained from FDTD modeling or the efficient boundary element method.<sup>[113]</sup> An important feature of these complex nanoparticle assemblies is the high field enhancement in hot spots, the gaps between nanoparticles, and their anisotropic optical response, shown in Figure 8d,e for chains composed of spherical and rod-shaped nanoparticles.<sup>[89,114]</sup> Linear plasmonic polymers are especially interesting for sub-wavelength information transport and light harvesting applications.<sup>[111]</sup> Controlling the degree of coupling between individual nanoparticles requires a precisely defined spacer material. The ligands used as spacers serve several functions simultaneously, because they provide colloidal stability in solution and during the self-assembly process, and they also keep the nanoparticles separated with controlled gaps after assembly.

Many methods are available and commonly used for depositing dispersions onto templates with chemical or topographical features such that the template will guide the self-assembly process. The remainder of this section is focused on techniques using templates to guide formation of plasmonic polymers. Templates are important for providing positional and orientation control of nanoparticles and for directing the shape of

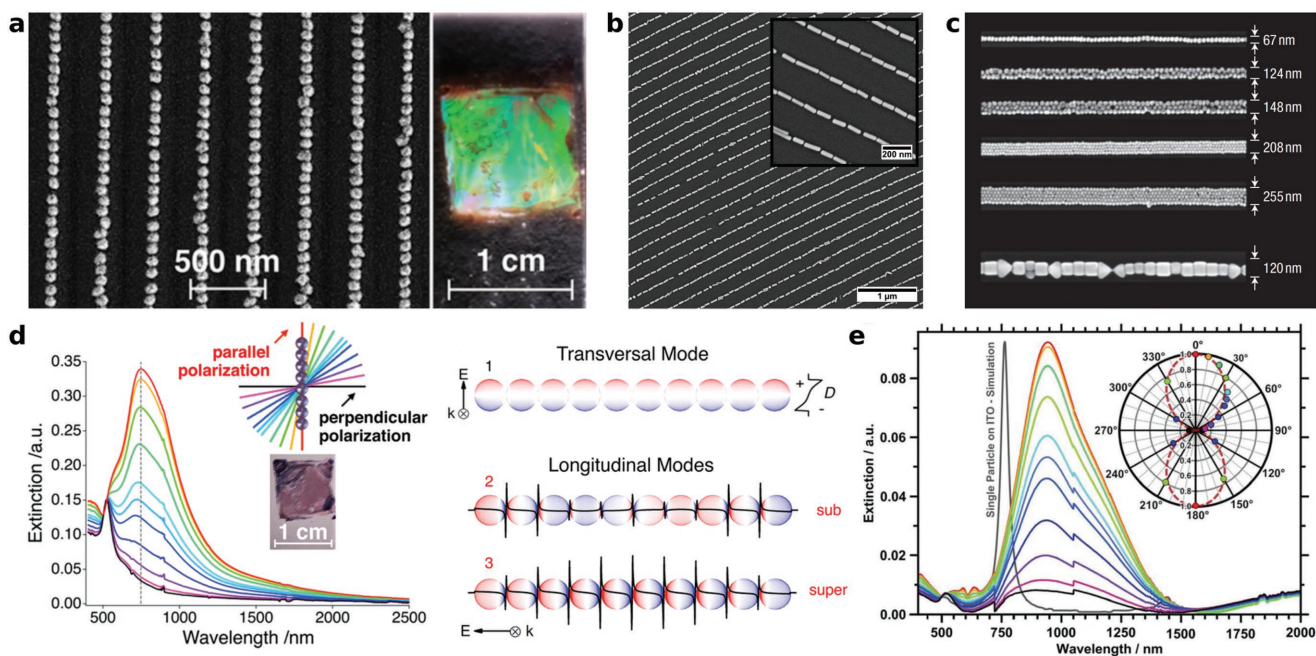


**Figure 8.** Structure and optical properties of plasmonic polymers. a) Periodic single particle lines from spin-coating and b) periodic nanorod lines from dip coating using wrinkled PDMS substrates as templates. c) Particle lines of varying thickness and morphologies by CAPA. d) Optical response and respective plasmonic modes of a linear quasi-infinite line of nanoparticles, as shown in (a), for different polarization angles. e) Optical response of linearly aligned gold nanorods as shown in (b). (a,d) Adapted with permission.<sup>[114]</sup> Copyright 2014, American Chemical Society. (b,e) Adapted under the terms of CC-BY license.<sup>[73]</sup> Copyright 2015, Royal Society of Chemistry. (c) Adapted with permission.<sup>[72c]</sup> Copyright 2007, Springer Nature.

the clusters into lines. Thus, the methods for assembling long linear chains of nanoparticles can be sorted from those that are highly scalable to those that provide the best positional control and allow assembly of the most complex geometries.

Spray coating is one of the most scalable methods for particle assembly and can be combined with templates to fabricate plasmonic polymers. The colloidal dispersion is sprayed onto the template and the colloids are assembled by chemical trapping or directed topographically.<sup>[115]</sup> Spraying with grazing incidence allows large-area fabrication of monolayers with optical anisotropy.<sup>[84,116]</sup>

In a drop casting, the colloidal dispersion is placed onto the template, confinement in the template provides the external trigger during the drying process for the assembly. The templates can have chemical binding sites and/or topographic traps.<sup>[74b,117]</sup> The control and reproducibility of drop-casting is limited, since the assembly process during drying is typically dictated by the uncontrolled laboratory environment.

Spin-coating, however, provides greater control over the drying rate and the amount of material deposited through setting the acceleration and rotational velocity. Highly regular and perfectly linear arrays of plasmonic polymers can be fabricated using centimeter-squared templates, as shown in Figure 8a.<sup>[114]</sup> Macroscopic wrinkled templates provide the required topography and do not limit the scalability of the assembly method, thus enabling conventional optical characterization of strong plasmonic effects.<sup>[89,114]</sup> Interparticle distances are similarly tuned *via* the spacer material.<sup>[74a]</sup> PNIPAm and protein coatings, depending on the targeted interparticle spacing, have proven suitable for self-assembly through spin-coating, because they impart high colloidal stability and can be used in the absence additional surfactants.<sup>[114,118]</sup> Spin-coating lacks orientational control of anisotropic nanoparticles, but dip coating is a closely related method that can give control over the orientation of nanoparticles.<sup>[119]</sup> In dip coating, the directed movement of the drying front allows orientation of anisotropic particles into the grooves of the templates by capillary forces, as shown for gold nanorods in Figure 8b.<sup>[89,98b]</sup>

As mentioned above, CAPA provides the most controlled assembly of plasmonic polymers. The well-controlled movement of the meniscus directs the colloids into the traps in the template. Consequently, a wide range of nanoparticle morphologies, nanoparticle sizes, and various materials of the dielectric shell are feasible to be assembled by CAPA. This is shown by Kraus et al. in Figure 8c for different sizes and for spherical as well as for cubic particles.<sup>[36b,72c]</sup> CAPA, however, relies on traps with exact and perfectly-matching geometry. Thus far, this demand is only fulfilled by lithographic methods like electron beam lithography, which typically lack cost-efficient scalability.

#### (IV) Plasmonic 2D ordered arrays

Finally, collective coupling of a 2D colloidal lattice can be achieved by long-range interactions between unit cells with domain sizes larger than the diffraction limit (i.e., several micrometers).<sup>[67]</sup> As a rule of thumb, coupling occurs between two gold nanoparticles when their separation is less than 2.5 times their diameter (or five times the diameter for silver

nanoparticles).<sup>[120]</sup> If the interparticle distances are too large to give plasmon coupling the plasmon resonance (broad band) can still couple to the first order Bragg diffraction resonance (narrow band), resulting in a surface lattice Fano resonance, as shown in Figure 9 (see also plasmonic symmetry breaking in Section 3).<sup>[121]</sup>

As discussed earlier, the lattice constant needs to cause first-order Bragg diffraction that energetically match the plasmon of the colloids for effective coupling. Therefore, the design relies on the precise packing of the self-assembled plasmonic building blocks into a plasmonic crystal. The experimental lattice constant is commonly defined by the thickness of the dielectric shell. Periodic nanoparticle monolayers can be prepared by spin-coating, dip coating or transfer of floating layers of nanoparticles from the liquid–air interface, e.g., via Langmuir–Blodgett or related systems.<sup>[78,121]</sup> These techniques result in close-packed lattices as shown in Figure 9a–c. For example, PVP and polystyrene (PS) support short interparticle distances, and for larger distances, PNIPAm has shown to be sufficiently surface-active due to its hydrophobicity for forming closed-packed plasmonic crystals when floating at the water–air interface.<sup>[78,122]</sup>

#### System integration via subsequent transfer

For many potential applications of functional plasmonic metasurfaces, integrating nanoparticle assemblies with other materials or systems is crucial. Two strategies are showing the greatest feasibility thus far, depending on the assembly method and the desired complexity. Either the template for self-assembly serves as the final substrate, or the self-assembled unit cells need to be transferred onto another “target” structure. As a general rule for transfer processes, the target substrate needs to be “stickier” than the template.<sup>[118b]</sup> This stickiness can be realized under wet and dry  $\mu$ -contact printing conditions and can be practically achieved through various approaches, including hydrophilic–hydrophobic interactions,<sup>[123]</sup> selective physis- or chemisorption of the dielectric spacer itself, addition of an adhesive promoter (e.g., polyethylenimine),<sup>[72c,89,114,124]</sup> or transfer into a polymer heated above its glass-transition temperature (e.g., poly(methyl methacrylate)).<sup>[36b]</sup>

## 4. Conclusion and Perspective: Smart Plasmonic Metasurfaces and Gain in Colloidal Plasmonic Metasurfaces

### 4.1. Mechanoplasmonic Metasurfaces

An intrinsic advantage of the colloidal approach toward plasmonic metasurfaces as compared to lithographic approaches is the compatibility with soft materials. While lithographic structures are typically formed on hard matter such as silicon wafers or metals films, colloidal nanoparticles can be easily assembled onto soft templates or be transferred onto soft materials after assembly by  $\mu$ -contact printing processes.<sup>[125]</sup> Transferring plasmonic metasurfaces into soft materials can enable mechanical tunability of plasmonic metasurfaces: interparticle distances or symmetries of particle assemblies can be changed by externally

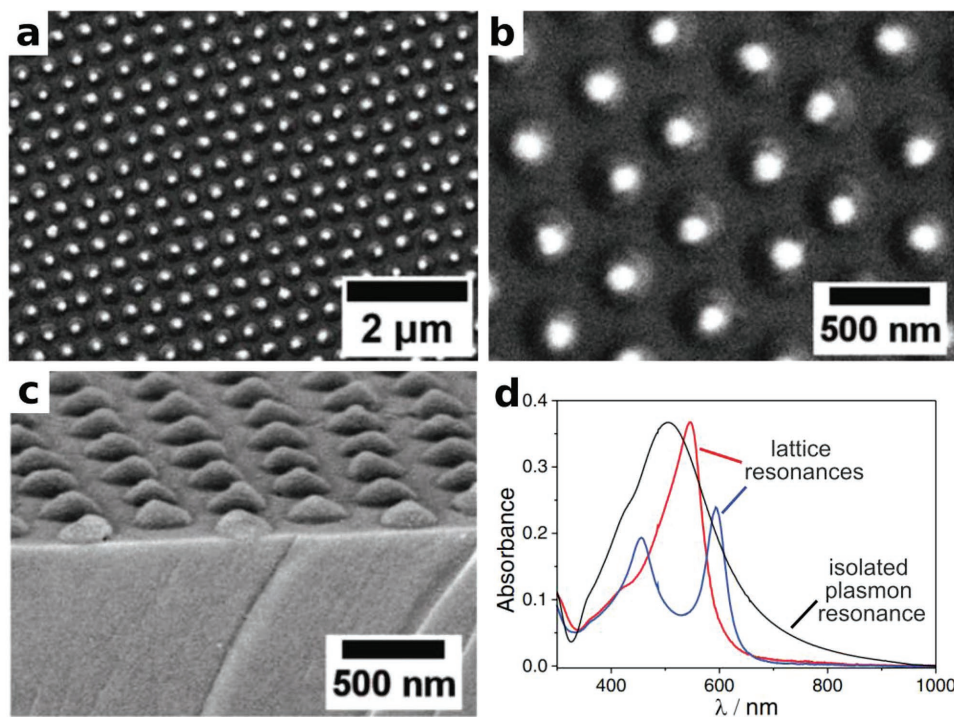


**Figure 9.** 2D lattices of plasmonic colloids supporting surface lattice resonances: a–c) SEM images of close-packed silver particles using PNIPAm as spacer material. d) Extinction spectra of isolated particles (black line), a close-packed nanoparticle film (red line) and index-matched close-packed particle film supporting a Fano resonance (blue line) due to the coupling of the Bragg lattice with the plasmon resonance. Adapted with permission.<sup>[121]</sup> Copyright 2017, Wiley-VCH.

applied strain. Indeed, one of the classical experiments for the demonstration of the plasmon ruler principle is based on a nanoparticle dimer on an elastomeric substrate and the systematic change of interparticle distance upon mechanical deformation, shown in **Figure 10a**.<sup>[126]</sup>

Stretching the substrate causes disrupt collective coupling effects, such as dividing extended lattices of plasmonic nanoparticles into smaller clusters, or even completely decoupling plasmonic nanoparticles. Optical properties can therefore be highly sensitive to mechanical deformation of the substrate. In work by Steiner et al.,<sup>[74a]</sup> an elastomeric substrate decorated with aligned plasmonic polymers with chain lengths above the infinite chain limit was mechanically stretched along the chain direction. Consequently, the plasmonic polymers ruptured into shorter plasmonic oligomers, which were shorter than the infinite chain limit (**Figure 10b**). Upon removing the applied stress, the optical properties changed reversibly to their initial state. While this effect is useful for strain sensing, a broader long-term application is mechanical modulation of optical properties.<sup>[127]</sup>

#### 4.2. Coherent Energy Transfer in Colloidal Plasmonic Metasurfaces

The concept of plasmonic nanoparticles can be further extended by considering each nanoparticle or nanoparticle assembly as a plasmonic resonator excited by a fluorescent emitter,<sup>[128]</sup> which makes large-scale, flexible, cost-efficient, and high-quality resonators readily available. When an emitter

comes in close contact to a plasmonic particle/assembly, the excitation is used for superior performance (such as faster decay rates, lower threshold and lower power consumption) in comparison to traditional photonic devices.<sup>[129]</sup> It is important to match the fluorescent emitter with the optical response of the plasmonic structures, as discussed in Sections 2 and 3 to observe coherent coupling effects. This optical response is expressed by the effective extinction cross-section of the target structure and for the UV–vis–NIR range, this is extensively covered by commercially available fluorescent emitters. Efficient coupling of light to the plasmon mode is important for distributing and directing energy. Near metal interfaces, the fluorophore couples nonradiatively and radiatively into decay channels, and increasing the decay rate causes a decrease in lifetime.<sup>[130]</sup> In a single particle-to-film coupled nanoantenna, radiative coupling processes can be studied systematically.<sup>[63c]</sup> There has been significant interest in particle-to-film coupling to understand weak and strong coupling scenarios, where the latter is also known as Rabi-splitting.<sup>[128]</sup> For chains of plasmonic nanoparticles, a fluorescent emitter at one end can excite all of the plasmon modes, both bright and dark modes (all of the energy eigenstates). The plasmon modes with high energies, also called subradiant modes, can suppress higher radiative losses in comparison to the energetically lowest mode, the super-radiant mode.<sup>[109]</sup> This property can then make chained assemblies useful as plasmonic waveguides for propagating energy across length scales below one micrometer with mode sizes smaller than the photon wavelength.<sup>[75]</sup> Alternatively, fluorescent emitters can coherently couple to the hybrid

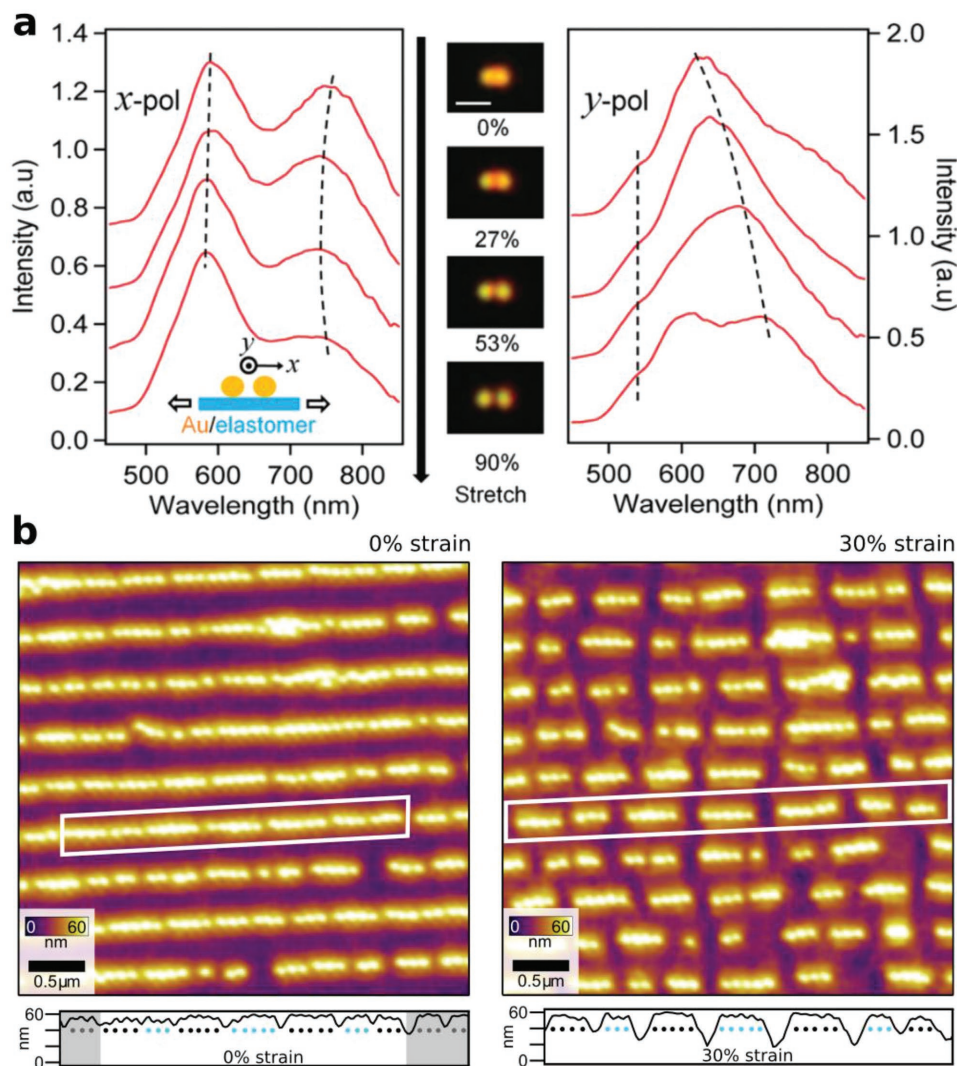


**Figure 10.** Beyond static plasmonic metasurfaces: mechanoplasmonic metasurfaces. a) Polarized scattering of a gold nanoparticle dimer, where stretching shifts the plasmon resonance for both longitudinal (left) and transverse (right) excitation. b) Reversible structural transition of quasi-infinite chains (plasmonic polymers) to plasmonic oligomers caused by mechanical deformation. (a) Adapted with permission.<sup>[126]</sup> Copyright 2010, American Chemical Society. (b) Adapted with permission.<sup>[174a]</sup> Copyright 2017, American Chemical Society.

plasmonic modes in a lattice assembly of plasmonic nanoparticles to generate lasing.<sup>[131]</sup>

#### 4.3. Conclusion

In conclusion, colloidal self-assembly has several distinct advantages over top-down fabrication methods for plasmonic metasurfaces. Plasmonic nanoparticles can be synthesized with stunningly well-defined shape and crystallinity, which is reflected in high optical quality on the single nanoparticle level. Template-assisted self-assembly approaches are scalable and energy efficient. Therefore, they merit consideration for further research and development of applications. Colloidal self-assembly is also a broad and highly general field that will continue contributing useful techniques for fabricating plasmonic metasurfaces. The mechanosensitive metasurfaces

discussed above are selected examples that illustrate the potential for developing mechanically tunable or active plasmonic metasurfaces. Achieving plasmonic metasurfaces with emergent properties requires establishing strong rational design strategies, where target nanoparticle shapes and self-assembled structures are established on the basis of modeling and simulation. Modeling can therefore guide the composition and shape of the target nanoparticles and the desired structures of the plasmonic metasurfaces formed through self-assembly. Structural and optical characterization can be used to assess the experiments and their match or mismatch with the anticipated results. This progress report summarizes the most important aspects and recent results for plasmonic metasurfaces, which will aid physicists in developing new concepts for optoelectronic structures with emergent properties and chemists as well as chemical engineers, who are advancing methods of wet-chemical synthesis and colloidal self-assembly.

## Acknowledgements

This project was financially supported by the Volkswagen Foundation through a Freigeist Fellowship to TAFK. The authors acknowledge the Deutsche Forschungsgemeinschaft (DFG) within the Cluster of Excellence "Center for Advancing Electronics Dresden" (cfaed) for financial support. The authors thank Joseph B. Tracy from the North Carolina State University, Charlene Ng, and Yannic Brasse for valuable discussion of the manuscript.

## Conflict of Interest

The authors declare no conflict of interest.

## Keywords

directed self-assembly, electromagnetic simulations, localized surface plasmon resonance, metasurfaces, nanoparticle synthesis

Received: April 30, 2018

Revised: August 17, 2018

Published online: September 17, 2018

- [1] H. Raether, *Surface Plasmons on Smooth and Rough Surfaces and on Gratings*, Springer Tracts in Modern Physics, Vol. 111, Springer, Berlin, Heidelberg **1988**, pp. 4–39.
- [2] S. Link, M. A. El-Sayed, *J. Phys. Chem. B* **1999**, *103*, 8410.
- [3] K. A. Willets, R. P. Van Duyne, *Annu. Rev. Phys. Chem.* **2007**, *58*, 267.
- [4] a) N. J. Halas, S. Lal, W.-S. Chang, S. Link, P. Nordlander, *Chem. Rev.* **2011**, *111*, 3913; b) M. Rycenga, C. M. Cobley, J. Zeng, W. Li, C. H. Moran, Q. Zhang, D. Qin, Y. Xia, *Chem. Rev.* **2011**, *111*, 3669.
- [5] S. J. Tan, L. Zhang, D. Zhu, X. M. Goh, Y. M. Wang, K. Kumar, C.-W. Qiu, J. K. W. Yang, *Nano Lett.* **2014**, *14*, 4023.
- [6] M. Karg, T. A. F. König, M. Retsch, C. Stelling, P. M. Reichstein, T. Honold, M. Thelakkat, A. Fery, *Mater. Today* **2015**, *18*, 185.
- [7] J. A. Schuller, E. S. Barnard, W. Cai, Y. C. Jun, J. S. White, M. L. Brongersma, *Nat. Mater.* **2010**, *9*, 193.
- [8] X. Huang, I. H. El-Sayed, W. Qian, M. A. El-Sayed, *J. Am. Chem. Soc.* **2006**, *128*, 2115.
- [9] K. M. Mayer, J. H. Hafner, *Chem. Rev.* **2011**, *111*, 3828.
- [10] P. K. Jain, W. Huang, M. A. El-Sayed, *Nano Lett.* **2007**, *7*, 2080.
- [11] J. M. Romo-Herrera, R. A. Alvarez-Puebla, L. M. Liz-Marzán, *Nanoscale* **2011**, *3*, 1304.
- [12] P. Nordlander, C. Oubre, E. Prodan, K. Li, M. I. Stockman, *Nano Lett.* **2004**, *4*, 899.
- [13] R. Kodyath, S. T. Malak, Z. A. Combs, T. Koenig, M. A. Mahmoud, M. A. El-Sayed, V. V. Tsukruk, *J. Mater. Chem. A* **2013**, *1*, 2777.
- [14] G. Veronis, S. Fan, in *Surface Plasmon Nanophotonics*, Springer Series in Optical Sciences, Vol. 131 (Eds: M. L. Brongersma, P. G. Kik), Springer Netherlands, Dordrecht **2007**, pp. 169–182.
- [15] A. V. Kildishev, A. Boltasseva, V. M. Shalaev, *Science* **2013**, *339*, 1232009.
- [16] Y. Zhao, A. Alù, *Phys. Rev. B* **2011**, *84*, 205428.
- [17] M. A. Schmidt, L. N. Prill Sempere, H. K. Tyagi, C. G. Poulton, P. S. J. Russell, *Phys. Rev. B* **2008**, *77*, 033417.
- [18] a) V. G. Veselago, *Sov. Phys. Usp.* **1968**, *10*, 509; b) R. A. Shelby, D. R. Smith, S. Schultz, *Science* **2001**, *292*, 77; c) J. Pendry, *Contemp. Phys.* **2004**, *45*, 191.
- [19] a) N. Fang, H. Lee, C. Sun, X. Zhang, *Science* **2005**, *308*, 534; b) J. B. Pendry, D. Schurig, D. R. Smith, *Science* **2006**, *312*, 1780; c) T. Ergin, N. Stenger, P. Brenner, J. B. Pendry, M. Wegener, *Science* **2010**, *328*, 337.
- [20] X. Ni, Z. J. Wong, M. Mrejen, Y. Wang, X. Zhang, *Science* **2015**, *349*, 1310.
- [21] W. Cai, V. Shalaev, *Optical Metamaterials*, Springer, New York, NY **2010**.
- [22] a) M. Mayer, A. M. Steiner, F. Röder, P. Formanek, T. A. F. König, A. Fery, *Angew. Chem., Int. Ed.* **2017**, *56*, 15866; b) M. Mayer, A. M. Steiner, F. Röder, P. Formanek, T. A. F. König, A. Fery, *Angew. Chem.* **2017**, *129*, 16082.
- [23] M. B. Müller, C. Kuttner, T. A. F. König, V. V. Tsukruk, S. Förster, M. Karg, A. Fery, *ACS Nano* **2014**, *8*, 9410.
- [24] J. J. Mock, D. R. Smith, S. Schultz, *Nano Lett.* **2003**, *3*, 485.
- [25] M. Mayer, L. Scarabelli, K. March, T. Altantzis, M. Tebbe, M. Kociak, S. Bals, F. J. García de Abajo, A. Fery, L. M. Liz-Marzán, *Nano Lett.* **2015**, *15*, 5427.
- [26] V. Myroshnychenko, J. Rodríguez-Fernández, I. Pastoriza-Santos, A. M. Funston, C. Novo, P. Mulvaney, L. M. Liz-Marzán, F. J. García de Abajo, *Chem. Soc. Rev.* **2008**, *37*, 1792.
- [27] C. Mätzler, **2002**.
- [28] P. B. Johnson, R. W. Christy, *Phys. Rev. B* **1972**, *6*, 4370.
- [29] M. N. Polyanskiy, Refractive index database, <https://refractiveindex.info> (accessed: April 2018).
- [30] a) J. Turkevich, P. C. Stevenson, J. Hillier, *Discuss. Faraday Soc.* **1951**, *11*, 55; b) N. G. Bastús, J. Comenge, V. Puntès, *Langmuir* **2011**, *27*, 11098.
- [31] G. González-Rubio, P. Díaz-Núñez, A. Rivera, A. Prada, G. Tardajos, J. González-Izquierdo, L. Bañares, P. Llombart, L. G. Macdowell, M. Alcolea Palafox, L. M. Liz-Marzán, O. Peña-Rodríguez, A. Guerrero-Martínez, *Science* **2017**, *358*, 640.
- [32] N. R. Jana, L. Gearheart, C. J. Murphy, *Langmuir* **2001**, *17*, 6782.
- [33] G. González-Rubio, T. M. de Oliveira, T. Altantzis, A. La Porta, A. Guerrero-Martínez, S. Bals, L. Scarabelli, L. M. Liz-Marzán, *Chem. Commun.* **2017**, *53*, 11360.
- [34] Y. Zheng, X. Zhong, Z. Li, Y. Xia, *Part. Part. Syst. Charact.* **2014**, *31*, 266.
- [35] a) L. Scarabelli, M. Coronado-Puchau, J. J. Giner-Casares, J. Langer, L. M. Liz-Marzán, *ACS Nano* **2014**, *8*, 5833; b) K. Park, H. Koerner, R. A. Vaia, *Nano Lett.* **2010**, *10*, 1433; c) N. R. Jana, *Chem. Commun.* **2003**, 1950.
- [36] a) V. Flauraud, M. Mastrangeli, G. D. Bernasconi, J. Butet, D. T. L. Alexander, E. Shahrabi, O. J. F. Martin, J. Brugger, *Nat. Nanotechnol.* **2016**, *12*, 73; b) A. Rey, G. Billardon, E. Lörtscher, K. Moth-Poulsen, N. Stühr-Hansen, H. Wolf, T. Bjørnholm, A. Stemmer, H. Riel, *Nanoscale* **2013**, *5*, 8680; c) L. Vigderman, B. P. Khanal, E. R. Zubarev, *Adv. Mater.* **2012**, *24*, 4811; d) L. Vigderman, E. R. Zubarev, *Chem. Mater.* **2013**, *25*, 1450.
- [37] M. J. Schnepf, M. Mayer, C. Kuttner, M. Tebbe, D. Wolf, M. Dulle, T. Altantzis, P. Formanek, S. Förster, S. Bals, T. A. F. König, A. Fery, *Nanoscale* **2017**, *9*, 9376.
- [38] Note: Continuation of plasmonic design principles.
- [39] Y. Xia, Y. Xiong, B. Lim, S. E. Skrabalak, *Angew. Chem., Int. Ed.* **2009**, *48*, 60.
- [40] S. E. Lohse, N. D. Burrows, L. Scarabelli, L. M. Liz-Marzán, C. J. Murphy, *Chem. Mater.* **2014**, *26*, 34.
- [41] a) L. Scarabelli, A. Sánchez-Iglesias, J. Pérez-Juste, L. M. Liz-Marzán, *J. Phys. Chem. Lett.* **2015**, *6*, 4270; b) S. Jessl, M. Tebbe, L. Guerrini, A. Fery, R. A. Alvarez-Puebla, N. Pazos-Perez, *Small* **2018**, *14*, 1703879; c) M. Tebbe, C. Kuttner, M. Mayer, M. Maennel, N. Pazos-Perez, T. A. F. König, A. Fery, *J. Phys. Chem. C* **2015**, *119*, 9513.
- [42] J. Zeng, Y. Zheng, M. Rycenga, J. Tao, Z.-Y. Li, Q. Zhang, Y. Zhu, Y. Xia, *J. Am. Chem. Soc.* **2010**, *132*, 8552.

- [43] a) S. Gómez-Graña, B. Goris, T. Altantzis, C. Fernández-López, E. Carbó-Argibay, A. Guerrero-Martínez, N. Almora-Barrios, N. López, I. Pastoriza-Santos, J. Pérez-Juste, S. Bals, G. Van Tendeloo, L. M. Liz-Marzán, *J. Phys. Chem. Lett.* **2013**, *4*, 2209; b) Q. Zhang, W. Li, C. Moran, J. Zeng, J. Chen, L.-P. Wen, Y. Xia, *J. Am. Chem. Soc.* **2010**, *132*, 11372.
- [44] S. Zhang, K. Bao, N. J. Halas, H. Xu, P. Nordlander, *Nano Lett.* **2011**, *11*, 1657.
- [45] Lumerical Inc., CA, <http://www.lumerical.com/tcad-products/fdtd/> (accessed: April 2018).
- [46] H.-J. Hagemann, W. Gudat, C. Kunz, *J. Opt. Soc. Am.* **1975**, *65*, 742.
- [47] B. T. Draine, P. J. Flatau, *J. Opt. Soc. Am. A* **1994**, *11*, 1491.
- [48] M. Born, E. Wolf, *Principles of Optics: Electromagnetic Theory of Propagation, Interference and Diffraction of Light*, 7th (expanded) ed., Cambridge University Press, Cambridge **2002**.
- [49] M. G. Moharam, T. K. Gaylord, *J. Opt. Soc. Am.* **1981**, *71*, 811.
- [50] R. Yu, L. M. Liz-Marzán, F. J. García de Abajo, *Chem. Soc. Rev.* **2017**, *46*, 6710.
- [51] S. Zhou, J. Li, K. D. Gilroy, J. Tao, C. Zhu, X. Yang, X. Sun, Y. Xia, *ACS Nano* **2016**, *10*, 9861.
- [52] F. Wang, Y. R. Shen, *Phys. Rev. Lett.* **2006**, *97*, 206806.
- [53] N. Liu, H. Giessen, *Angew. Chem., Int. Ed.* **2010**, *49*, 9838.
- [54] X. Zhuo, X. Zhu, Q. Li, Z. Yang, J. Wang, *ACS Nano* **2015**, *9*, 7523.
- [55] S. Song, X. Ma, M. Pu, X. Li, K. Liu, P. Gao, Z. Zhao, Y. Wang, C. Wang, X. Luo, *Adv. Opt. Mater.* **2017**, *5*, 1600829.
- [56] J.-H. Choi, Y.-S. No, J.-P. So, J. M. Lee, K.-H. Kim, M.-S. Hwang, S.-H. Kwon, H.-G. Park, *Nat. Commun.* **2016**, *7*, 11569.
- [57] M. Mesch, T. Weiss, M. Schäferling, M. Hentschel, R. S. Hegde, H. Giessen, *ACS Sens.* **2018**, *3*, 960.
- [58] S. Simoncelli, Y. Li, E. Cortés, S. A. Maier, *Nano Lett.* **2018**, *18*, 3400.
- [59] B. Luk'yanchuk, N. I. Zheludev, S. A. Maier, N. J. Halas, P. Nordlander, H. Giessen, C. T. Chong, *Nat. Mater.* **2010**, *9*, 707.
- [60] Y. S. Joe, A. M. Satanin, C. S. Kim, *Phys. Scr.* **2006**, *74*, 259.
- [61] T. König, R. Kodyath, Z. A. Combs, M. A. Mahmoud, M. A. El-Sayed, V. V. Tsukruk, *Part. Part. Syst. Charact.* **2014**, *31*, 274.
- [62] C. Ng, J. J. Cadusch, S. Dligatch, A. Roberts, T. J. Davis, P. Mulvaney, D. E. Gómez, *ACS Nano* **2016**, *10*, 4704.
- [63] a) R. Chikkaraddy, B. de Nijs, F. Benz, S. J. Barrow, O. A. Scherman, E. Rosta, A. Demetriadou, P. Fox, O. Hess, J. J. Baumberg, *Nature* **2016**, *535*, 127; b) A. Rose, T. B. Hoang, F. McGuire, J. J. Mock, C. Ciraci, D. R. Smith, M. H. Mikkelsen, *Nano Lett.* **2014**, *14*, 4797; c) M. J. Schnepf, Y. Brasse, F. R. Goßler, A. M. Steiner, J. Obermeier, M. Lippitz, A. Fery, T. A. F. König, *Z. Phys. Chem.* **2018**, *232*, 1593.
- [64] a) R. A. Alvarez-Puebla, A. Agarwal, P. Manna, B. P. Khanal, P. Aldeanueva-Potel, E. Carbo-Argibay, N. Pazos-Perez, L. Vigderman, E. R. Zubarev, N. A. Kotov, L. M. Liz-Marzán, *Proc. Natl. Acad. Sci. USA* **2011**, *108*, 8157; b) S. Jaber, M. Karg, A. Morfa, P. Mulvaney, *Phys. Chem. Chem. Phys.* **2011**, *13*, 5576; c) J. A. Lopez-Sanchez, N. Dimitratos, C. Hammond, G. L. Brett, L. Kesavan, S. White, P. Miedziak, R. Tiruvalam, R. L. Jenkins, A. F. Carley, D. Knight, C. J. Kiely, G. J. Hutchings, *Nat. Chem.* **2011**, *3*, 551.
- [65] E. Prodan, C. Radloff, N. J. Halas, P. Nordlander, *Science* **2003**, *302*, 419.
- [66] L.-Y. Wang, K. W. Smith, S. Dominguez-Medina, N. Moody, J. M. Olson, H. Zhang, W.-S. Chang, N. Kotov, S. Link, *ACS Photonics* **2015**, *2*, 1602.
- [67] J. P. S. Fitzgerald, M. Karg, *Phys. Status Solidi* **2017**, *214*, 1600947.
- [68] D. Khlopin, F. Laux, W. P. Wardley, J. Martin, G. A. Wurtz, J. Plain, N. Bonod, A. V. Zayats, W. Dickson, D. Gérard, *J. Opt. Soc. Am. B* **2017**, *34*, 691.
- [69] C. Stelling, C. R. Singh, M. Karg, T. A. F. König, M. Thelakkat, M. Retsch, *Sci. Rep.* **2017**, *7*, 42530.
- [70] a) W. Zhou, M. Dridi, J. Y. Suh, C. H. Kim, D. T. Co, M. R. Wasielewski, G. C. Schatz, T. W. Odom, *Nat. Nanotechnol.* **2013**, *8*, 506; b) A. I. Väkeväinen, R. J. Moerland, H. T. Rekola, A.-P. Eskelinen, J.-P. Martikainen, D.-H. Kim, P. Törmä, *Nano Lett.* **2014**, *14*, 1721.
- [71] M. Grzelczak, J. Vermant, E. M. Furst, L. M. Liz-Marzán, *ACS Nano* **2010**, *4*, 3591.
- [72] a) N. Gaponik, S. G. Hickey, D. Dorfs, A. L. Rogach, A. Eychmüller, *Small* **2010**, *6*, 1364; b) T. Kraus, D. Brodoceanu, N. Pazos-Perez, A. Fery, *Adv. Funct. Mater.* **2013**, *23*, 4529; c) T. Kraus, L. Malaquin, H. Schmid, W. Riess, N. D. Spencer, H. Wolf, *Nat. Nanotechnol.* **2007**, *2*, 570; d) A. Guerrero-Martínez, J. Pérez-Juste, E. Carbó-Argibay, G. Tardajos, L. M. Liz-Marzán, *Angew. Chem., Int. Ed.* **2009**, *48*, 9484.
- [73] a) J. Lee, J.-H. Huh, K. Kim, S. Lee, *Adv. Funct. Mater.* **2018**, *28*, 1707309; b) S. J. Tan, M. J. Campolongo, D. Luo, W. Cheng, *Nat. Nanotechnol.* **2011**, *6*, 268.
- [74] a) A. M. Steiner, M. Mayer, M. Seuss, S. Nikolov, K. D. Harris, A. Alexeev, C. Kuttner, T. A. F. König, A. Fery, *ACS Nano* **2017**, *11*, 8871; b) L. S. Slaughter, B. A. Willingham, W.-S. Chang, M. H. Chester, N. Ogden, S. Link, *Nano Lett.* **2012**, *12*, 3967; c) J. A. Fan, K. Bao, L. Sun, J. Bao, V. N. Manoharan, P. Nordlander, F. Capasso, *Nano Lett.* **2012**, *12*, 5318.
- [75] F. N. Gür, C. P. T. McPolin, S. Raza, M. Mayer, D. J. Roth, A. M. Steiner, M. Löffler, A. Fery, M. L. Brongerma, A. V. Zayats, T. A. F. König, T. L. Schmidt, **2017**, arXiv:1712.09141 [physics.optics].
- [76] S. Ni, H. Wolf, L. Isa, *Langmuir* **2018**, *34*, 2481.
- [77] a) M. Tebbe, C. Kuttner, M. Männel, A. Fery, M. Chanana, *ACS Appl. Mater. Interfaces* **2015**, *7*, 5984; b) M. Karg, T. Hellweg, P. Mulvaney, *Adv. Funct. Mater.* **2011**, *21*, 4668.
- [78] K. Volk, J. P. S. Fitzgerald, M. Retsch, M. Karg, *Adv. Mater.* **2015**, *27*, 7332.
- [79] a) J.-W. Jeon, P. A. Ledin, J. A. Geldmeier, J. F. Ponder, M. A. Mahmoud, M. El-Sayed, J. R. Reynolds, V. V. Tsukruk, *Chem. Mater.* **2016**, *28*, 2868; b) M. Karg, I. Pastoriza-Santos, J. Pérez-Juste, T. Hellweg, L. M. Liz-Marzán, *Small* **2007**, *3*, 1222; c) E. W. Edwards, M. Chanana, D. Wang, H. Möhwald, *Angew. Chem., Int. Ed.* **2008**, *47*, 320; d) M. Chanana, P. Rivera-Gil, M. A. Correa-Duarte, L. M. Liz-Marzán, W. J. Parak, *Angew. Chem., Int. Ed.* **2013**, *52*, 4179.
- [80] a) M. A. Noginov, G. Zhu, A. M. Belgrave, R. Bakker, V. M. Shalaev, E. E. Narimanov, S. Stout, E. Herz, T. Suteewong, U. Wiesner, *Nature* **2009**, *460*, 1110; b) S. Cormier, T. Ding, V. Turek, J. J. Baumberg, *Adv. Opt. Mater.* **2018**, *6*, 1701281; c) B. Reiser, L. González-García, I. Kanelidis, J. H. M. Maurer, T. Kraus, *Chem. Sci.* **2016**, *7*, 4190.
- [81] L. Malaquin, T. Kraus, H. Schmid, E. Delamarche, H. Wolf, *Langmuir* **2007**, *23*, 11513.
- [82] a) D. Nepal, M. S. Onses, K. Park, M. Jespersen, C. J. Thode, P. F. Nealey, R. A. Vaia, *ACS Nano* **2012**, *6*, 5693; b) A. Klinkova, H. Thérien-Aubin, A. Ahmed, D. Nykypanchuk, R. M. Choueiri, B. Gagnon, A. Muntyanu, O. Gang, G. C. Walker, E. Kumacheva, *Nano Lett.* **2014**, *14*, 6314; c) Q. Chen, S. C. Bae, S. Granick, *Nature* **2011**, *469*, 381; d) G. González-Rubio, J. González-Izquierdo, L. Bañares, G. Tardajos, A. Rivera, T. Altantzis, S. Bals, O. Peña-Rodríguez, A. Guerrero-Martínez, L. M. Liz-Marzán, *Nano Lett.* **2015**, *15*, 8282.
- [83] M. N. Sanz-Ortiz, K. Sentosun, S. Bals, L. M. Liz-Marzán, *ACS Nano* **2015**, *9*, 10489.
- [84] P. T. Probst, S. Sekar, T. A. F. König, P. Formanek, G. Decher, A. Fery, M. Pauly, *ACS Appl. Mater. Interfaces* **2018**, *10*, 3046.
- [85] C. Hanske, G. González-Rubio, C. Hamon, P. Formentín, E. Modin, A. Chuvilin, A. Guerrero-Martínez, L. F. Marsal, L. M. Liz-Marzán, *J. Phys. Chem. C* **2017**, *121*, 10899.

- [86] a) F. N. Gür, F. W. Schwarz, J. Ye, S. Diez, T. L. Schmidt, *ACS Nano* **2016**, *10*, 5374; b) V. A. Turek, R. Chikkaraddy, S. Cormier, B. Stockham, T. Ding, U. F. Keyser, J. J. Baumberg, *Adv. Funct. Mater.* **2018**, *28*, 1706410.
- [87] A. P. Lane, X. Yang, M. J. Maher, G. Blachut, Y. Asano, Y. Someya, A. Mallavarapu, S. M. Sirard, C. J. Ellison, C. G. Willson, *ACS Nano* **2017**, *11*, 7656.
- [88] E.-M. Park, J. Choi, B. H. Kang, K.-Y. Dong, Y. Park, I. S. Song, B.-K. Ju, *Thin Solid Films* **2011**, *519*, 4220.
- [89] M. Tebbe, M. Mayer, B. A. Glatz, C. Hanske, P. T. Probst, M. B. Müller, M. Karg, M. Chanana, T. A. F. König, C. Kuttner, A. Fery, *Faraday Discuss.* **2015**, *181*, 243.
- [90] a) J. Guasch, J. Diemer, H. Riahinezhad, S. Neubauer, H. Kessler, J. P. Spatz, *Chem. Mater.* **2016**, *28*, 1806; b) J. Deng, C. Zhao, J. P. Spatz, Q. Wei, *ACS Nano* **2017**, *11*, 8282.
- [91] M. Pretzl, A. Schweikart, C. Hanske, A. Chiche, U. Zettl, A. Horn, A. Böker, A. Fery, *Langmuir* **2008**, *24*, 12748.
- [92] a) Z. Liu, T. Chang, H. Huang, T. He, *RSC Adv.* **2013**, *3*, 20464; b) S. Sanwaria, S. Singh, A. Horechyy, P. Formanek, M. Stamm, R. Srivastava, B. Nandan, *RSC Adv.* **2015**, *5*, 89861.
- [93] S. B. Darling, *Prog. Polym. Sci.* **2007**, *32*, 1152.
- [94] a) A. Schweikart, A. Fery, *Microchim. Acta* **2009**, *165*, 249; b) A. Schweikart, A. Horn, A. Böker, A. Fery, in *Complex Macromolecular Systems I*, Vol. 227 (Eds: A. H. E. Müller, H.-W. Schmidt), Springer, Berlin, Heidelberg **2009**, pp. 75–99.
- [95] B. A. Glatz, M. Tebbe, B. Kaoui, R. Aichele, C. Kuttner, A. E. Schedl, H.-W. Schmidt, W. Zimmermann, A. Fery, *Soft Matter* **2015**, *11*, 3332.
- [96] O. Nicoletti, F. de la Peña, R. K. Leary, D. J. Holland, C. Ducati, P. A. Midgley, *Nature* **2013**, *502*, 80.
- [97] H. Chen, L. Shao, T. Ming, K. C. Woo, Y. C. Man, J. Wang, H.-Q. Lin, *ACS Nano* **2011**, *5*, 6754.
- [98] a) H. Wang, K. O’Dea, L. Wang, *Opt. Lett.* **2014**, *39*, 1457; b) M. Mayer, M. Tebbe, C. Kuttner, M. J. Schnepf, T. A. F. König, A. Fery, *Faraday Discuss.* **2016**, *191*, 159; c) Y. Brasse, M. B. Müller, M. Karg, C. Kuttner, T. A. F. König, A. Fery, *ACS Appl. Mater. Interfaces* **2018**, *10*, 3133.
- [99] T. B. Hoang, G. M. Akselrod, C. Argyropoulos, J. Huang, D. R. Smith, M. H. Mikkelsen, *Nat. Commun.* **2015**, *6*, 7788.
- [100] T. A. F. König, P. A. Ledin, J. Kerszulis, M. A. Mahmoud, M. A. El-Sayed, J. R. Reynolds, V. V. Tsukruk, *ACS Nano* **2014**, *8*, 6182.
- [101] J. B. Lassiter, F. McGuire, J. J. Mock, C. Ciraci, R. T. Hill, B. J. Wiley, A. Chilkoti, D. R. Smith, *Nano Lett.* **2013**, *13*, 5866.
- [102] T. A. F. König, P. A. Ledin, M. Russell, J. A. Geldmeier, M. A. Mahmoud, M. A. El-Sayed, V. V. Tsukruk, *Nanoscale* **2015**, *7*, 5230.
- [103] J. Clara-Rahola, R. Contreras-Caceres, B. Sierra-Martin, A. Maldonado-Valdivia, M. Hund, A. Fery, T. Hellweg, A. Fernandez-Barbero, *Colloids Surf., A* **2014**, *463*, 18.
- [104] a) Y. Zheng, T. Thai, P. Reineck, L. Qiu, Y. Guo, U. Bach, *Adv. Funct. Mater.* **2013**, *23*, 1519; b) H. Cha, J. H. Yoon, S. Yoon, *ACS Nano* **2014**, *8*, 8554.
- [105] a) N. J. Greybush, I. Liberal, L. Malassis, J. M. Kikkawa, N. Engheta, C. B. Murray, C. R. Kagan, *ACS Nano* **2017**, *11*, 2917; b) T. Chen, B. M. Reinhard, *Adv. Mater.* **2016**, *28*, 3522.
- [106] S. Ni, J. Leemann, H. Wolf, L. Isa, *Faraday Discuss.* **2015**, *181*, 225.
- [107] E.-M. Roller, L. V. Besteiro, C. Pupp, L. K. Khorashad, A. O. Govorov, T. Liedl, *Nat. Phys.* **2017**, *13*, 761.
- [108] *Macromolecule (Polymer Molecule)*, IUPAC Compendium of Chemical Terminology (Eds: M. Nič, J. Jiráč, B. Košata, A. Jenkins, A. McNaught), IUPAC, Research Triangle Park, NC **2009**.
- [109] B. Willingham, S. Link, *Opt. Express* **2011**, *19*, 6450.
- [110] L. S. Slaughter, L.-Y. Wang, B. A. Willingham, J. M. Olson, P. Swanglap, S. Dominguez-Medina, S. Link, *Nanoscale* **2014**, *6*, 11451.
- [111] S. J. Barrow, D. Rossouw, A. M. Funston, G. A. Botton, P. Mulvaney, *Nano Lett.* **2014**, *14*, 3799.
- [112] W. Cai, R. Sainidou, J. Xu, A. Polman, F. J. García de Abajo, *Nano Lett.* **2009**, *9*, 1176.
- [113] a) U. Hohenester, *Comput. Phys. Commun.* **2014**, *185*, 1177; b) F. J. García de Abajo, A. Howie, *Phys. Rev. B* **2002**, *65*.
- [114] C. Hanske, M. Tebbe, C. Kuttner, V. Bieber, V. V. Tsukruk, M. Chanana, T. A. F. König, A. Fery, *Nano Lett.* **2014**, *14*, 6863.
- [115] S. Sekar, V. Lemaire, H. Hu, G. Decher, M. Pauly, *Faraday Discuss.* **2016**, *191*, 373.
- [116] H. Hu, M. Pauly, O. Felix, G. Decher, *Nanoscale* **2017**, *9*, 1307.
- [117] N. Pazos-Pérez, W. Ni, A. Schweikart, R. A. Alvarez-Puebla, A. Fery, L. M. Liz-Marzán, *Chem. Sci.* **2010**, *1*, 174.
- [118] a) M. Mueller, M. Tebbe, D. V. Andreeva, M. Karg, R. A. Alvarez Puebla, N. Pazos Perez, A. Fery, *Langmuir* **2012**, *28*, 9168; b) A. Castelli, A. Striolo, A. Roig, C. Murphy, J. Reguera, L. Liz-Marzán, A. Mueller, K. Critchley, Y. Zhou, M. Brust, A. Thill, L. Scarabelli, L. Tadiello, T. A. F. König, B. Reiser, M. A. López-Quintela, M. Buzza, A. Deák, C. Kuttner, E. Gonzalez Solveyra, L. Pasquato, D. Portehault, H. Mattoussi, N. A. Kotov, E. Kumacheva, K. Heatley, J. Bergueiro, G. González, W. Tong, M. N. Tahir, B. Abécassis, O. Rojas-Carrillo, Y. Xia, M. Mayer, D. Peddis, *Faraday Discuss.* **2016**, *191*, 229.
- [119] J. Huang, A. R. Tao, S. Connor, R. He, P. Yang, *Nano Lett.* **2006**, *6*, 524.
- [120] S. K. Ghosh, T. Pal, *Chem. Rev.* **2007**, *107*, 4797.
- [121] K. Volk, J. P. S. Fitzgerald, P. Ruckdeschel, M. Retsch, T. A. F. König, M. Karg, *Adv. Opt. Mater.* **2017**, *5*, 1600971.
- [122] a) J. Henzie, M. Grünwald, A. Widmer-Cooper, P. L. Geissler, P. Yang, *Nat. Mater.* **2011**, *11*, 131; b) K. J. Si, D. Sikdar, Y. Chen, F. Eftekhari, Z. Xu, Y. Tang, W. Xiong, P. Guo, S. Zhang, Y. Lu, Q. Bao, W. Zhu, M. Premaratne, W. Cheng, *ACS Nano* **2014**, *8*, 11086; c) M. T. Perez Cardenas, C. Kong, J. He, S. Litvin, M. L. Meyerson, Z. Nie, *ACS Nano* **2018**, *12*, 1107.
- [123] C. Hanske, M. B. Müller, V. Bieber, M. Tebbe, S. Jessl, A. Wittemann, A. Fery, *Langmuir* **2012**, *28*, 16745.
- [124] a) M. Müller, M. Karg, A. Fortini, T. Hellweg, A. Fery, *Nanoscale* **2012**, *4*, 2491; b) C. Kuemin, L. Nowack, L. Bozano, N. D. Spencer, H. Wolf, *Adv. Funct. Mater.* **2012**, *22*, 702.
- [125] a) X. Zhu, L. Shi, X. Liu, J. Zi, Z. Wang, *Nano Res.* **2010**, *3*, 807; b) U. Cataldi, R. Caputo, Y. Kurylyak, G. Klein, M. Chekini, C. Umeton, T. Bürgi, *J. Mater. Chem. C* **2014**, *2*, 7927; c) M. G. Millyard, F. Min Huang, R. White, E. Spigone, J. Kivioja, J. J. Baumberg, *Appl. Phys. Lett.* **2012**, *100*, 073101; d) Y.-L. Chiang, C.-W. Chen, C.-H. Wang, C.-Y. Hsieh, Y.-T. Chen, H.-Y. Shih, Y.-F. Chen, *Appl. Phys. Lett.* **2010**, *96*, 041904; e) L. Gao, Y. Zhang, H. Zhang, S. Doshay, X. Xie, H. Luo, D. Shah, Y. Shi, S. Xu, H. Fang, J. A. Fan, P. Nordlander, Y. Huang, J. A. Rogers, *ACS Nano* **2015**, *9*, 5968.
- [126] F. Huang, J. J. Baumberg, *Nano Lett.* **2010**, *10*, 1787.
- [127] a) D. Wang, M. R. Bourgeois, W.-K. Lee, R. Li, D. Trivedi, M. P. Knudson, W. Wang, G. C. Schatz, T. W. Odom, *Nano Lett.* **2018**, *18*, 4549; b) A. Yang, A. J. Hryn, M. R. Bourgeois, W.-K. Lee, J. Hu, G. C. Schatz, T. W. Odom, *Proc. Natl. Acad. Sci. USA* **2016**, *113*, 14201.
- [128] J. T. Hugall, A. Singh, N. F. van Hulst, *ACS Photonics* **2018**, *5*, 43.
- [129] S. Wang, X.-Y. Wang, B. Li, H.-Z. Chen, Y.-L. Wang, L. Dai, R. F. Oulton, R.-M. Ma, *Nat. Commun.* **2017**, *8*, 1889.
- [130] J. R. Lakowicz, Y. Fu, *Laser Photonics Rev.* **2009**, *3*, 221.
- [131] D. Wang, W. Wang, M. P. Knudson, G. C. Schatz, T. W. Odom, *Chem. Rev.* **2018**, *118*, 2865.